



2 Title: A multi-model assessment of the early last deglaciation (PMIP4 LDv1): The
meltwater paradox reigns supreme

Corresponding author: Brooke Snoll¹

4 Email for correspondence: ee19b2s@leeds.ac.uk

6 Co-authors: Ruza Ivanovic¹, Lauren Gregoire¹, Sam Sherriff-Tadano¹, Laurie Menviel², Takashi
Obase³, Ayako Abe-Ouchi³, Nathaëlle Bouttes⁴, Chengfei He⁵, Feng He⁶, Marie Kapsch⁷, Uwe
Mikolajewicz⁷, Juan Muglia⁸, Paul Valdes⁹

8 Affiliations: ¹University of Leeds, ²Climate Change Research Centre, University of New South Wales
Sydney, ³University of Tokyo, ⁴LSCE, ⁵University of Miami, ⁶Univeristy of Wisconsin, ⁷Max Planck
10 Institute for Meteorology, ⁸CESIMAR, ⁹University of Bristol

12

14

16

18

20

22

24

26



28 Abstract

30 Transient simulations of the last deglaciation have been increasingly performed to better understand
31 the processes leading to both the overall deglacial climate trajectory as well as the centennial- to
32 decadal- scale climate variations prevalent during deglaciations. The Paleoclimate Modelling
33 Intercomparison Project (PMIP) has provided a framework for an internationally coordinated effort
34 in simulating the last deglaciation (~20 – 11 ka BP) whilst encompassing a broad range of models.
35 Here, we present a multi-model intercomparison of 17 simulations of the early part of the last
36 deglaciation (~20 – 15 ka BP) from nine different climate models spanning a range of model
37 complexities and uncertain boundary conditions/forcings.

38 A main contrasting element between the simulations is the method by which groups
39 implement freshwater fluxes from the melting ice sheets and how this forcing then impacts ocean
40 circulation and surface climate. We find that the choice of meltwater scenario heavily impacts the
41 deglacial climate evolution, but the response of each model depends largely on the sensitivity of the
42 model to the freshwater forcing as well as to other aspects of the experimental design (e.g., CO₂
43 forcing or ice sheet reconstruction). There is agreement throughout the ensemble that warming
44 begins in the high latitudes associated with increasing insolation and delayed warming in the tropics
45 aligned with the later increases in atmospheric CO₂ concentration. The delay in this warming in the
46 tropics is dependent on the timescale of the CO₂ reconstruction used by the modelling group.
47 Simulations with freshwater forcings greater than 0.1 Sverdrup (Sv) after 18 ka BP experience
48 delayed warming in the North Atlantic, whereas simulations with smaller freshwater forcings begin
49 deglaciating sooner. All simulations show a strong correlation between North Atlantic temperatures,
50 atmospheric CO₂ concentrations, and the AMOC. In simulations with a freshwater forcing greater than
51 0.1 Sv, North Atlantic temperatures correlate strongly with changes in the AMOC. Simulations with a
52 smaller freshwater forcing show stronger correlations with atmospheric CO₂. This indicates that the
53 amount of meltwater strongly controls the climate trajectory of the deglaciation. Comparing multiple
54 simulations run by the same model demonstrate model biases by showing similar surface climate
55 spatial patterns despite the use of different ice sheet reconstructions and/or meltwater flux
56 scenarios. Simulations run with different models, but similar boundary conditions, have provided
57 insight into the sensitivity of individual models to particular forcings, such as the amount freshwater
58 forcing, which has been highly debated in previous studies.

59 This debate has stemmed from the so-called 'meltwater paradox' that exists in choosing how
60 much meltwater to input into simulations of the last deglaciation (i.e., large and geologically
61 inconsistent meltwater forcings that successfully produce abrupt climate events versus



glaciologically realistic meltwater fluxes that do not). The results of this research highlight how
62 important this decision is.

1. Introduction

64 At the onset of the most recent deglaciation, ~19 thousand years before present (ka BP), ice sheets
that covered the Northern Hemisphere at the Last Glacial Maximum (LGM; Dyke 2004; Lambeck et al.
66 2014; Hughes et al. 2016) started to melt (Gregoire et al. 2012), Earth began to warm (Jouzel et al.
2007; Buizert et al. 2014), and sea levels rose (Lambeck et al. 2014). Known as the *last deglaciation*,
68 this time period is defined by major, long-term (order of ten thousand years) climate transitions from
the most recent cold glacial to the current warm interglacial state, as well as many short-term, decadal
70 to centennial-scale warmings and coolings of more than 5 °C (de Beaulieu and Reille 1992;
Severinghaus and Brook 1999; Lea et al. 2003; Buizert et al. 2014). These short-term abrupt
72 temperature changes are often also accompanied by sudden reorganisations of basin-wide ocean
circulations (e.g., Roberts et al. 2010; Ng et al. 2018) and jumps in sea level of tens of meters in a few
74 hundred years (e.g., Deschamps et al. 2012; Lambeck et al. 2014).

Abrupt climate changes observed in the early last deglaciation such as the Greenland cold
76 period known as Heinrich Stadial 1 (between ~18.5 and 14.7 ka BP; Broecker and Putnam 2012;
Huang et al. 2014, 2019; Crivellari et al. 2018; Ng et al. 2018) and the Bølling Warming (an abrupt
78 warming that occurs ~14.7 ka BP in Greenland at the end of Heinrich Stadial 1; Severinghaus and
Brook 1999; Lea et al. 2003; Buizert et al. 2014), are often attributed to changes in the Atlantic
80 meridional overturning circulation (AMOC). The strength and structure of the ocean circulation is a
key control on the North Atlantic and Arctic climate and is dependent on the stratification of the water
82 layers in crucial convection sites in the North Atlantic (Lynch-Stieglitz et al. 2007; McCarthy et al.
2017). When the AMOC is strong, more heat is transported towards the North Atlantic causing
84 regional warming in Greenland and the North Atlantic (Rahmstorf 2002).

There is debate on the strength of the LGM AMOC and how this initial state impacts the
86 preceding climate change of the deglaciation. Previous observations (e.g., Lynch-Stieglitz et al. 2007;
Böhm et al. 2015; Lynch-Stieglitz 2017) suggest a weaker and shallower AMOC than present-day
88 during the LGM, whilst more recent modelling studies show a deep and strong ocean circulation (e.g.,
Menviel et al. 2011; He et al. 2021; Sherriff-Tadano and Klockmann 2021; Kapsch et al. 2022; Snoll et al.
90 al. 2022) due to the presence of thick ice sheets (Oka et al. 2012; Sherriff-Tadano et al. 2018; Galbraith
and de Lavergne 2019). Multiple more recent data assimilation modelling studies (e.g., Menviel et al.
92 2012, 2017; Muglia and Schmittner 2021; Wilmes et al. 2021; Pöppelmeier et al. 2023b) have shown



agreement with previous observations by reproducing a weak and shallower LGM AMOC relative to
94 the pre-industrial or Holocene. However, several ocean circulation proxy studies (e.g., McManus et al.
2004; Gherardi et al. 2005, 2009; Ivanovic et al. 2016; Ng et al. 2018), using the $^{231}\text{Pa}/^{230}\text{Th}$ ratio,
96 demonstrate some consensus of a vigorous but shallower AMOC coming out of the LGM (relative to
the modern day) that subsequently weakened and shallowed (but remained active; Bradtmiller et al.
98 2014; Repschläger et al. 2021; Pöppelmeier et al. 2023b) during the abrupt transition to Heinrich
Stadial 1. Palaeoproxy records (e.g., McManus et al. 2004; Lynch-Stieglitz 2017; Ng et al. 2018) and
100 modelling studies (e.g., Liu et al. 2009; Menviel et al. 2011; He et al. 2021) suggest that the ocean
circulation strength remains weak until its rapid resumption at the end of the stadial, when the
102 Bølling Warming occurs.

The AMOC pattern can be perturbed easily by several climate feedbacks. For example, if
104 freshwater is deposited into the critical convection sites in the subpolar North Atlantic, i.e., the
Labrador Sea and Nordic Seas, locations of high sensitivity to wind patterns and sea ice formation,
106 the circulation strength can be disrupted (Rahmstorf 1999). Evidence from several sites report sea
level rise, and therefore a freshwater flux, as early in the deglaciation as 19.5 ka BP, attributed to
108 widespread retreat of Northern Hemisphere ice sheets in response to an increase in northern latitude
summer insolation (Yokoyama et al. 2000; Clarke et al. 2009). Carlson and Clark (2012) concluded
110 that the LGM was terminated by a rapid 5 – 10 meters sea level rise between 19.5 and 19 ka BP, and
sea levels rose a further 8 – 20 meters from ~19 to 14.5 ka BP with the melt of the Laurentide and
112 Eurasian ice sheets. More recent reconstructions of sea level and ice volume change suggest a similar
view with ~10-15 meters of sea level rise between the end of the LGM (~21 – 20 ka BP) and 18 ka BP
114 and an additional ~25 meters before 14.5 ka BP (Lambeck et al. 2014; Peltier et al. 2015; Roy and
Peltier 2018; Gorbarenko et al. 2022). In some cases where meltwater fluxes are applied to the North
116 Atlantic in model simulations, rapid decreases of up to 10 °C in temperature occur, resembling the
transition to Heinrich Stadial 1 (e.g., Ganopolski and Rahmstorf 2001; Knutti et al. 2004; Brown and
118 Galbraith 2016; Menviel et al. 2020).

Transient simulations of the last deglaciation have been increasingly performed to better
120 understand the multi-millennial scale processes and the shorter and more dramatic climate changes
by examining dynamic and threshold behaviours (Braconnot et al. 2012), determining the effects of
122 temporally varying climate forcings, and identifying what mechanisms in the model can cause
recorded climate signals (see section 1.2 by Ivanovic et al. (2016) and examples therein). In turn,
124 these simulations also provide us with the opportunity to test the ability of models to simulate climate



126 processes and interactions as well as different hypotheses for drivers of change (i.e., climate triggers,
interactions, and feedbacks).

128 One particularly challenging aspect in the experimental design of last deglaciation
simulations is prescribing ice sheet evolution and the resultant freshwater flux and sea level rise.
130 Notwithstanding the qualitative rationale for why ocean-bound meltwater disrupts ocean circulation
and climate (McManus et al. 2004; Clarke et al. 2009; Thornalley et al. 2010), it has been recently
132 argued that climate models are too sensitive to freshwater fluxes under some conditions. For example,
data reconstructions suggest only a small change in AMOC ~11.7 to 6 ka BP, whereas CCSM3
134 simulated a greater response to the freshwater forcing associated with the final Northern
Hemisphere deglaciation at this time (He and Clark 2022), when sea level rose by 50 meters during
this interval (Lambeck et al. 2014; Cuzzone et al. 2016; Ullman et al. 2016). This result may be quite
136 model dependent, and we note that others had previously suggested the converse: that model
responses to freshwater (and other) forcings could be too muted, from what we understand of past
138 climate change (Valdes 2011). Certainly, to disrupt climate in a Heinrich Stadial-like way, many
previous glacial simulations have required quite large meltwater fluxes compared to what may be
140 inferred from geological records (Kageyama et al. 2013). This remains an interesting point of
contention, and certainly some models no longer appear as 'stable' as they once did. Moreover, the
142 sensitivity of the North Atlantic Ocean circulation to glacial melting is poorly constrained.

144 There are, however, strong indications that the impact of oceanic freshwater fluxes is highly
dependent on the location that they enter the ocean (depth and latitude/longitude), as it determines
the efficiency of convection disruption (e.g., Roche et al. 2007, 2010; Smith and Gregory 2009; Otto-
146 Bliesner and Brady 2010; Condron and Winsor 2012; Ivanovic et al. 2017; Romé et al. 2022). Similarly,
the background climate and ocean state may also be important for how responsive ocean circulation
148 is to freshwater forcing—e.g., whether AMOC is already strong and deep or weak and shallow (Bitz et
al. 2007; Schmittner and Lund 2014; Dome Fuji Ice Core Project Members: et al. 2017; Pöppelmeier
150 et al. 2023a), or specifically where deep water formation occurs (Smith and Gregory 2009; Roche et
al. 2010). The choice of a model's boundary conditions in the palaeo setting (e.g., ice sheet geometry)
152 can influence its sensitivity to freshwater perturbation (e.g., compare the results of Romé et al. (2022)
with those of Ivanovic et al. (2018)—Romé's low freshwater forced LGM simulations have an
154 oscillating AMOC, whereas Ivanovic's do not—different ice sheet reconstructions are used in both;
and see Kapsch et al. (2022) who simulate the last deglaciation testing the climate response to
156 different ice sheet reconstructions). Ice sheet geometry specifically has been demonstrated to be
linked with AMOC strength due to the effect of ice sheet height on surface winds and wind-driven



158 gyres, which can increase the northward transport of salty waters. Multiple model studies (e.g.,
160 Ullman et al. 2014; Löfverström and Lora 2017; Sherriff-Tadano et al. 2018; Kapsch et al. 2022) have
162 shown that a thicker Laurentide ice sheet results in a stronger AMOC. Hence, the influence of deglacial
ice sheet meltwater on AMOC is likely highly dependent on both the model, choice of boundary
conditions and forcings, and the initial ocean condition.

Previous modelling efforts (e.g., Liu et al. 2009; Roche et al. 2011; Menviel et al. 2011;
164 Gregoire et al. 2012) have performed transient simulations to learn more about the last deglaciation
and the interaction between ocean and atmosphere. Liu et al. (2009) were the first to publish a
166 synchronously coupled atmosphere-ocean general circulation model simulation of the last
deglaciation, henceforth referred to as *TraCE-21ka*. In this study, a freshwater flux was used to
168 regulate the AMOC to achieve a set of target ocean circulation, surface air temperature, and sea
surface temperature conditions as interpreted from a selection of proxy records in multiple locations
170 between the LGM and the onset of the Bølling Warming (see Fig. 1 by Liu et al. (2009)), preceded by
a switch to a geologic reconstruction of freshwater forcing (He 2011). Largely following the strategy
172 of *TraCE-21ka*, He et al. (2021) performed an updated version of the simulation with an isotope
enabled model, referred to as *iTraCE*. Similarly, they also implemented a freshwater flux tuned to their
174 interpretation of an ocean circulation proxy record (McManus et al. 2004) between the LGM and the
onset of the Bølling Warming and produced model output timeseries that very closely resemble water
176 isotope observations in Greenland (GISP2; Grootes et al. 1993), northern (Kulishu Cave; Ma et al.
2012) and southern China (Hulu Cave; Wang et al. 2001), and southern Asia (Mawmluh Cave; Dutt et
178 al. 2015). Menviel et al. (2011) adopted a similar approach, using freshwater fluxes tuned to ocean
circulation and climate records (McManus et al. 2004 and Alley 2000 respectively) in order to better
180 understand abrupt changes in the Southern Hemisphere and their possible link to the so-called bi-
polar seesaw (Broecker 1998; Stocker 1998) versus Antarctic melting.

182 The meltwater inputs used in each of these simulations, however, do not follow ice sheet
reconstructions (e.g., see Ivanovic et al., 2018). Instead, the meltwater fluxes are, on occasion over
184 twice as large as suggested by ICE-6G_C VM5a (henceforth 'ICE-6G_C'; Argus et al. 2014; Peltier et al.
2015) and GLAC-1D (Tarasov and Peltier 2002; Tarasov et al. 2012; Briggs et al. 2014; Ivanovic et al.
186 2016). Furthermore, the freshwater flux must then be shut off to reinvigorate the AMOC and instigate
the Bølling Warming, ending Heinrich Stadial 1, but this is at the same time as recorded rise in global
188 sea level of 12-22 meters in ~350 years or less, known as Meltwater Pulse 1a (Deschamps et al. 2012).
This creates a meltwater paradox, where the freshwater forcing required by models to produce



190 recorded climate change is broadly in opposition to the meltwater history reconstructed from ice
sheet and sea level records.

192 Simulations performed by Kapsch et al. (2022) and Snoll et al. (2022) add weight to this so-
called meltwater paradox. They use meltwater forcing scenarios in accordance with observable ice
194 volume change but have not been able to replicate the AMOC or surface air temperature proxy
records. Instead, the AMOC remains stronger than ocean circulation records suggest for Heinrich
196 Stadial 1, and the models simulate an abrupt *cooling* at ~14.5 ka BP instead of the *Bølling Warming*.

The picture is further confounded by Gregoire et al. (2012), who forced an ice sheet model
198 with a transient climate simulation of the last deglaciation that included meltwater pulses, such as
Meltwater Pulse 1a, but which did not experience major AMOC or surface temperature perturbations
200 as a result of the freshwater (e.g., see Fig. S2 by Gregoire et al. (2012)).

Similar simulations of the last deglaciation have been run with no prescribed meltwater or a
202 meltwater forcing that is applied as a global salinity adjustment (i.e., rather than localised surface
forcing). Without the use of the freshwater forcing, these simulations do not reproduce any abrupt
204 climate change events during the deglaciation. For instance, those described by Snoll et al. (2022) are
similarly not able to replicate the AMOC or surface air temperature proxy records, but also do not
206 simulate the abrupt cooling at ~14.5 ka BP and instead, display a gradual warming throughout the
deglaciation. Roche et al. (2011) performed a no-melt simulation of the last deglaciation that matches
208 closely with NGRIP temperatures (North Greenland Ice Core Project, 42.32° W, 75.01° N) until 16 ka
BP when Heinrich Stadial 1 is observed. Yet, at ~11 ka BP, after the abrupt events occur, the simulation
210 and NGRIP temperatures meet each other again. Bouttes et al. (2023) also conduct a no-melt as well
as meltwater forced simulation, but with an adaptation of the same model used by Roche et al. (2011).
212 Comparably, the new simulations also match closely with the NGRIP temperatures, but only until 17
ka BP, when they start to warm more rapidly and do not replicate Heinrich Stadial 1 cooling or the
214 subsequent *Bølling Warming*.

The simulation performed by Obase and Abe-Ouchi (2019), is unique in that it is able to
216 simulate a weak AMOC during the onset of the deglaciation and the *Bølling Warming* without
releasing (and then stopping) an unrealistically large amount of freshwater. Instead, they input a
218 gradually increasing amount of meltwater that remains at or below the level of ice volume loss in the
reconstruction. At ~14.7 ka BP, the AMOC and Greenland surface air temperature abruptly increases
220 due to the gradual warming of the Southern Ocean and increased formation of Antarctic Bottom
Water reaching a threshold whilst the meltwater flux in the North Atlantic is maintained, overcoming
222 the effect of the meltwater. This simulation still does not consider Meltwater Pulse 1a and has lower



224 than observed meltwater input before that point, yet it is distinctive in its ability to replicate a weak
ocean circulation in the early deglaciation and the Bølling Warming even with a continuous
freshwater flux.

226 Despite the decades of research simulating the last deglaciation and numerous observable
records of this time period, uncertainty still remains about the mechanisms that cause the recorded
228 climate signals as well as how to replicate them ‘realistically’ in model simulations, and therefore how
to unravel the meltwater paradox. Furthermore, CO₂ and orbital forcing are also shown to impact the
230 course of the deglaciation and the occurrence of abrupt climate changes (i.e., results shown by Oka et
al. 2012; Klockmann et al. 2016, 2018; Zhang et al. 2017; Sherriff-Tadano et al. 2018), and also
232 potentially modulate the sensitivity of the AMOC to freshwater fluxes (Obase and Abe-Ouchi 2019;
Sun et al. 2022). Liu et al. (2009) demonstrate that the warming in *TraCE-21ka* between 17 and 14.67
234 ka BP is dominated by the CO₂ forcing (over the orbital forcing; see their Fig. S6a), which coincides
with the first major rise of atmospheric CO₂ in their simulation. Whereas Gregoire et al. (2015) find,
236 using a couple climate-ice sheet model (FAMOUS-GLIMMER) and following the deglacial simulation
of Gregoire et al. (2012), that by 9 ka BP, orbital forcing caused 50% of the reduction in ice volume,
238 greenhouse gases 30%, and the interaction between the two caused the last 20% in their simulations.
Sun et al. (2022) shows the affect that these forcings have on the sensitivity of the AMOC with the use
240 of multiple sensitivity experiments from an Earth system model (COSMOS). Their experiments
demonstrate that a weak AMOC (in a Heinrich Stadial 1-like state, for example) is more likely to
242 recover (like that of the Heinrich Stadial 1 to Bølling Warming transition) with a higher atmospheric
CO₂ concentration, and that larger ice sheets result in a stronger AMOC that is less sensitive to
244 meltwater fluxes. These findings highlight the importance of solving the convolved issue of model
sensitivity to specific forcings/boundary conditions and the initial climate condition, and model
246 dependency of simulation results—the crux of the remaining unknowns.

248 The Paleoclimate Modelling Intercomparison Project (PMIP) has been internationally
coordinating multi-model simulations for over 30 years (Braconnot et al. 2007, 2012) to tackle such
unknowns. The PMIP working groups have developed protocols to facilitate the effort of simulating
250 past global climate changes by providing an outline of the model set-up to use (i.e., boundary
conditions and forcings), allowing for easier cross-model comparison and the international pooling
252 of resources to examine differing hypotheses to explain past climates, including uncertain model
inputs (such as forcings and boundary conditions). As part of PMIP4, the last deglaciation protocol
254 (Ivanovic et al. 2016) encompasses a broad range of models and is intentionally designed to be
flexible, in order to be a suitable technical and computational undertaking for all participants and to



256 allow exploration of different climate scenarios. Instead of one specific and rigid configuration for the
257 experiment design, modelling groups are given a choice of recommended forcings and boundary
258 conditions. Thus, analysing model output of multiple simulations of the last deglaciation provides the
259 opportunity to look at differences between experimental designs and their impact on the onset of the
260 deglaciation using different models, though it can also be challenging. For example, it is difficult to
261 compare directly different model results in a strict 'benchmarking' (Braconnot et al. 2012; Harrison
262 et al. 2015) framework, and there may be mismatched ranges of forcing within which to examine
263 model sensitivities. However, to some extent this is already the case for transient simulations, even if
264 a strictly singular protocol is applied, as initial conditions or simulated events can impact later results,
265 such as the starting AMOC condition or whether an abrupt cooling did or did not occur. Furthermore,
266 the technical implementation of boundary conditions/forcings in different models also leads to
267 discrepancies in their configuration.

268 The Coupled Model Intercomparison Project (CMIP) has set a precedent for how to analyse
269 ensembles of simulations with inconsistent experimental designs, such as those testing different
270 Shared Socioeconomic Pathways (SSPs), and the more recent incorporation of PMIP simulations in
271 CMIP has allowed for a better understanding of model biases and therefore, how to better compare
272 their output. In addition, past flexible protocols and 'ensembles of opportunity' comprising
273 simulations of contrasting model boundary conditions and forcings (e.g., Schmidt et al. 2012; Lunt et
274 al. 2012; Kageyama et al. 2013) have shown the value of experiment design flexibility for
275 understanding climate change in a multi-model framework without committing all resources to
276 specific paradigms. In short, it can be scientifically advantageous for groups to have the opportunity
277 to determine their own focus whilst still contributing computationally expensive and technically
278 challenging simulations towards an overarching, multi-model aim of learning more about physical
279 behaviours in response to different simulated scenarios.

280 This study compares 17 simulations of the last deglaciation from nine different climate
281 models with dissimilar experimental designs. Our aim is to take advantage of the numerous
282 simulations available to better understand the chain of events and mechanisms of climate changes in
283 the early last deglaciation (i.e., from 20 to 15 ka BP), and our collective ability to simulate them. We
284 focus on the early deglaciation because although models may start differently from the LGM, the
285 divergence from each other is smaller in comparison to further into the deglaciation. We investigate
286 the similarities and differences between the model results and what aspects of the variations in the
287 model output can be attributed to the experimental design or model biases by analysing the transition
288 from the LGM, when and where the warming starts, and the impact of freshwater forcing. We also



290 address the meltwater paradox by discussing the results of meltwater scenario choices made by the
291 modelling groups.

2. Experiment designs across the ensemble

292 *Table 1: Detail of simulations referenced in the multi-model intercomparison.*

Model	Resolution	Simulation Reference Name	Publication (model; simulation)	Simulation Duration (ka BP)	Prescribed Ice Sheet	GHG	Meltwater Scenario
CCSM3	Atmosphere: 2.8° with 26 levels Ocean: 1° x 0.3° with 25 levels	<i>TraCE-21ka</i>	Collins et al. 2006; Liu et al. 2009	22 – 0	ICE-5G	Joos and Spahni 2008	<i>TraCE-21ka</i>
FAMOUS	Atmosphere: 7.5° x 5° with 11 levels Ocean: 3.75° x 2.5° with 20 levels	<i>FAMOUS</i>	Smith et al. 2008; Gregoire et al. 2012	20 – 13	ICE-5G	Based on PMIP2; see Harrison et al. (2002)	<i>Bespoke</i> (Fig. 1f)
HadCM3B	Atmosphere: 3.75° x 2.5° with 19 levels Ocean: 1.25° with 20 levels	<i>HadCM3_uniform</i>	Valdes et al. 2017; Snoll et al. 2022 and this study	23 – 2 ka CE	ICE-6G_C	Loulergue et al. 2008; Schilt et al. 2010; Bereiter et al. 2015	<i>Melt-uniform</i>
		<i>HadCM3_routed</i>					<i>Melt-routed</i>
		<i>HadCM3_TraCE</i>					<i>TraCE-like</i>
iCESM	Atmosphere: 2.5° x 1.9° with 30 levels Ocean: 1° with 60 levels	<i>iTraCE</i>	Hurrell et al. 2013; He et al. 2021	21 – 11	ICE-6G_C	Lüthi et al. 2008	<i>TraCE-like</i>
iLOVECLIM	Atmosphere: 5.6° with 3 vertical levels Ocean: 3° with 20 levels	<i>iLOVE_uniform_ice6gc</i>	Goosse et al. 2010; Bouttes et al. 2022	21 – 9	ICE-6G_C	Loulergue et al. 2008; Schilt et al. 2010; Bereiter et al. 2015	<i>Melt-uniform</i>
		<i>iLOVE_routed_ice6gc</i>					<i>Melt-routed</i>
		<i>iLOVE_uniform_glac</i>			GLAC-1D		<i>Melt-uniform</i>
		<i>iLOVE_routed_glac</i>					<i>Melt-routed</i>
LOVECLIM	Atmosphere: 5.6° with 3 vertical levels Ocean: 3° with 20 levels, dynamic vegetation model	<i>LOVECLIM</i>	Goosse et al. 2010; This study, but similar to simulations by Menviel et al. (2011)	21 – 11.8	ICE-5G	Köhler et al. 2017	<i>TraCE-like</i>
MIROC	Atmosphere: 2.8° with 20 levels Ocean: 1.4° with 43 levels	<i>MIROC</i>	Hasumi and Emori 2004; Obase and Abe-Ouchi 2019	21 – 13	ICE-6G_C	Loulergue et al. 2008; Schilt et al. 2010; Bereiter et al. 2015	<i>Bespoke</i> (gradual increase)
MPI-ESM-CR	Atmosphere: 3.75° with 31 levels Ocean: 3° with 40 levels	<i>MPI_global_ice6gc</i>	Giorgetta et al. 2013; Kapsch et al. 2022	26 – 0	ICE-6G_C	Köhler et al. 2017	<i>Melt-uniform</i> (Global meltwater flux)
		<i>MPI_routed_ice6gc</i>					<i>Melt-routed</i>
		<i>MPI_routed_glac</i>			GLAC-1D		<i>Melt-routed</i>
UVic	Atmosphere: 3.6° x 1.8° Ocean: 3.6° x 1.8° with 19 levels	<i>UVic_shorthosing</i>	Weaver et al. 2001; This study, but based on LGM simulations by Muglia and Schmittner (2015, 2021)	21 – 14	ICE-6G_C	dynamic	<i>Bespoke</i>
		<i>UVic_longhosing</i>					

294 The comparison presented here is based on 17 simulations produced independently by eight
295 different palaeoclimate modelling groups, using nine different climate models (Table 1). Most groups
296 have followed the most recent PMIP4 last deglaciation protocol for their experimental design, while
others use older publications for boundary conditions or a more *bespoke* configuration depending on



298 their own modelling goals. The simulations from HadCM3, LOVECLIM, iLOVECLIM, iCESM, MIROC,
and MPI modelling groups use greenhouse gas configurations on the AICC2012 age model of Veres et
300 al. (2013) (Fig. 1b). *FAMOUS* and *TraCE-21ka* use an older age model in which the deglacial rise in CO₂
starts one thousand years later. All simulations prescribe insolation following Berger (1978). The
302 PMIP4 last deglaciation protocol recommends using the GLAC-1D (Ivanovic et al., 2016) and/or ICE-
6G_C (Peltier et al., 2015) ice sheet reconstructions. HadCM3, iCESM, MIROC and UVic modelling
304 groups opted for ICE-6G_C, MPI and iLOVECLIM simulations use both ICE-6G_C and GLAC1-D, and
FAMOUS, *LOVECLIM*, and *TraCE-21ka* use the older ICE-5G (Peltier 2004).

306 Freshwater forcing across the ensemble is more complex. The PMIP4 last deglaciation
protocol recommends two different meltwater scenarios (*melt-routed* and *melt-uniform*) based on ice
308 volume change as calculated from the ice sheet reconstruction chosen by the modelling group (GLAC-
1D and ICE-6G_C are recommended). The *melt-uniform* scenario is a globally uniform freshwater flux
310 or salinity adjustment through time applied throughout the whole ocean to conserve water mass
during deglaciation of the ice sheets, whereas the *melt-routed* scenario is a distributed routing that
312 gives the flux of freshwater through time at individual meltwater river outlets along the coast
(Ivanovic et al. 2016; Riddick et al. 2018 - used by MPI).

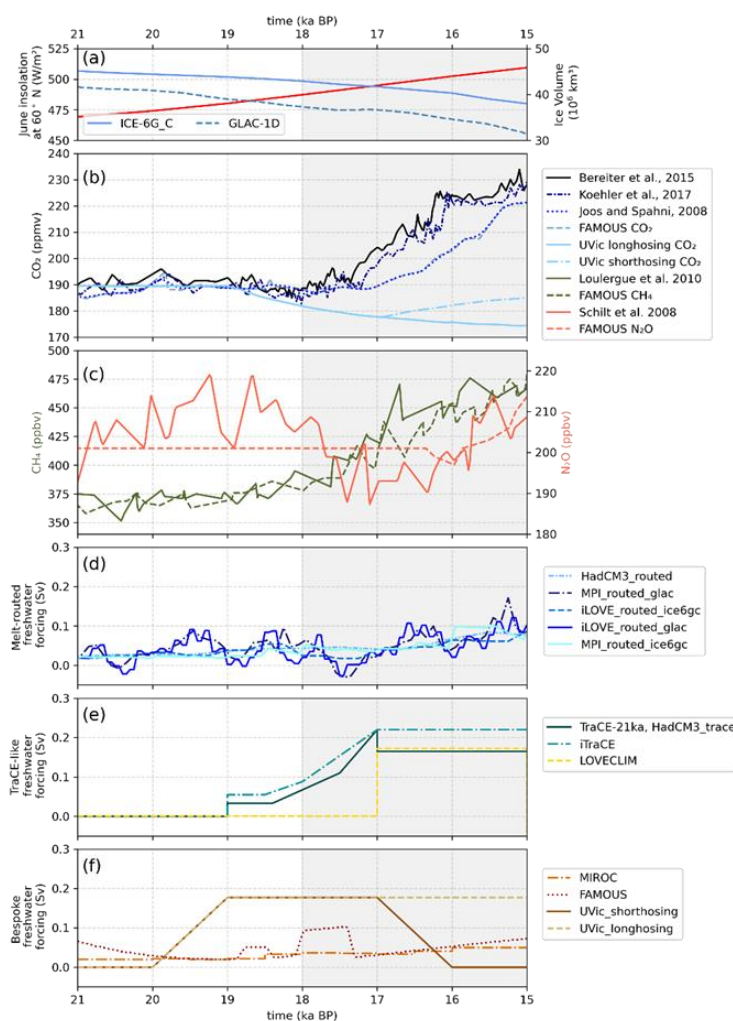
314 Because a large discrepancy between the simulations is the prescribed freshwater flux
scenario (Fig. 1c-e), and ice sheet meltwater fluxes are known to have a major impact on ocean
316 circulation and climate (see above), the simulations have been grouped into four categories based on
their meltwater forcing: *melt-routed*, *melt-uniform*, those based on the *TraCE-21ka A* simulation
318 (henceforth referred to as '*TraCE-like*'; Liu et al. 2009), and '*bespoke*' scenarios that fall outside of the
other three categories. Within these categories, however, there is variation in how the freshwater
320 forcing is derived from the ice sheet reconstruction as well as in the technical implementation of the
chosen meltwater scenario (for example, for the *melt-routed* and *melt-uniform* scenarios, see Wickert
322 2016, section 2.2.2 for HadCM3; Kapsch et al. 2022; section 2 for MPI; Bouttes et al. 2022, section 2.4
for iLOVECLIM). For the *melt-routed* simulations, the modelling groups then release the calculated
324 meltwater flux to ocean grid cells according to the distribution calculated by the individual groups'
drainage network models (see respective papers). For the *melt-uniform* simulations, HadCM3 and
326 iLOVECLIM modelling groups apply a globally uniform freshwater flux throughout the entire volume
of the ocean, whereas the MPI modelling group applies a freshwater flux at the surface of the ocean
328 or land. Because of this nuance, the MPI *melt-uniform* simulation is instead labelled as a 'global
surface meltwater flux' but is still placed in the *melt-uniform* category for our analysis.



330 We somewhat over-simplistically refer to PMIP4 meltwater scenarios as ‘realistic’, because
they are based on the chosen ice sheet reconstruction prescribed in the simulation. Nonetheless, it is
332 important to note that the precise history of the meltwater flux (distribution and rates) remains quite
uncertain, as hinted at by differences in the reconstructions. Between 20 and 15 ka BP, the ‘realistic’
334 freshwater flux according to ICE-6G_C does not exceed 0.1 Sv and that according to GLAC-1D only
exceeds 0.1 Sv as it nears Meltwater Pulse 1a.

336 In the *TraCE-like* simulations, the strategy of prescribing freshwater to induce an inferred
AMOC history requires the freshwater flux to reach nearly 0.2 Sv or greater—twice the ‘realistic’
338 amount based on sea level records (Fig. 1d; Carlson and Clark 2012; Lambeck et al. 2014).

For the *bespoke-freshwater* cluster of simulations, *MIROC* implements a gradually increasing
340 flux that always remains below the ‘realistic’ values. *FAMOUS* uses a reconstructed flux based on an
earlier estimate from sea level records (produced as part of the ORMEN project; more information
342 provided by Gregoire (2010)), which follows the more up-to-date ice sheet reconstructions relatively
closely except when a larger freshwater flux is applied at two points during Heinrich Stadial 1
344 (between 19 and 17 ka BP; corresponding to the acceleration of Northern Hemisphere ice loss, as
noted by Carlson and Clarke, 2012, and the melt of the Eurasian ice sheet as reconstructed by Hughes
346 et al. (2016)). The UVic simulations use a total freshwater flux calculated as three times the sea level
changes reconstructed by Lambeck et al. (2014); one scenario where the freshwater flux is applied
348 between 19 and 15 ka BP (*Uvic_longhosing*) and one where the flux is only applied between 19 and
17 ka BP (*Uvic_shorthosing*; Table 1).



350

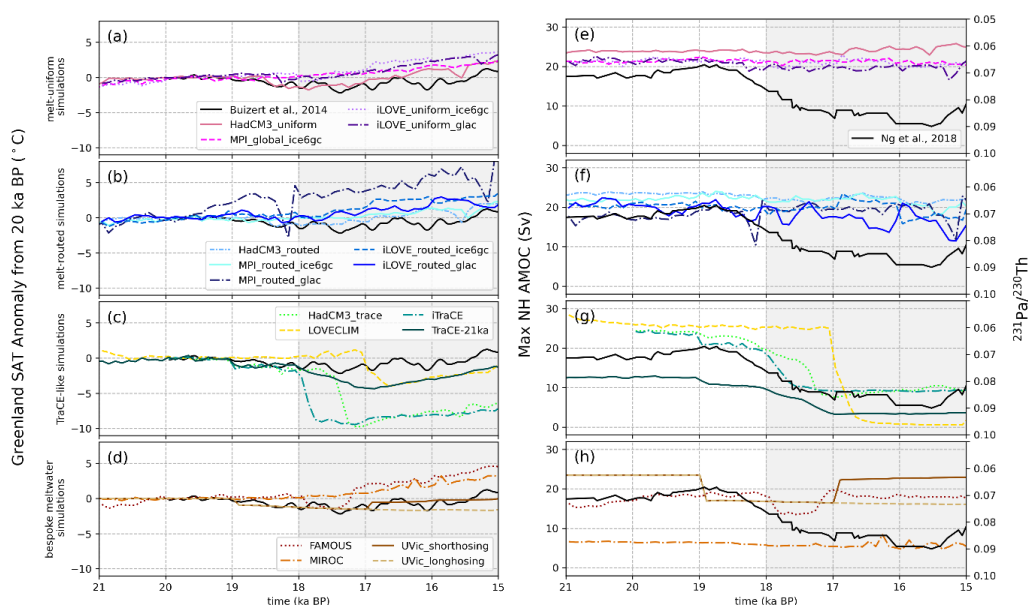
352 *Fig. 1: Climate forcings for the simulations. (a) Ice volume loss since the Last Glacial Maximum (LGM; 21 ka BP) as part of the*
 353 *ICE-6G_C ice sheet reconstruction (Argus et al., 2014; Peltier et al., 2015) and the GLAC-1D ice sheet reconstruction (Tarasov*
 354 *and Peltier 2002; Tarasov et al. 2012; Briggs et al. 2014; Ivanovic et al. 2016). (b) Atmospheric greenhouse gas*
 355 *concentrations dependent on simulation set-up. (d)-(f) Freshwater flux (Sv) for simulations with imposed meltwater. Melt-*
 356 *uniform simulations have the same total meltwater flux into the global ocean as melt-routed simulations (d), but in melt-*
 357 *uniform scenarios, the freshwater is spread through the entire ocean or across the whole ocean surface (see main text) rather*
 358 *than at point sources and hence are so diluted/uniformly distributed as to have limited direct forcing power.*

358

360 The UVic simulations include a dynamic carbon cycle model with prognostic atmospheric CO₂ aiming to replicate the sedimentary records of deep ocean carbon. The freshwater flux is, therefore, tuned to replicate the AMOC structure associated with these sedimentary records, but the location of



362 the meltwater input is based on plume positions like those of the HadCM3 simulations. The UVic
 363 simulations are included in the broader comparisons presented here (i.e., Fig. 3 Fig. 5). However,
 364 because of their uniqueness of experiment design and motivation, the differences between the UVic
 365 simulations and the wider multi-model ensemble are too great for a more detailed comparison of
 366 results, and they are therefore omitted from further analysis and discussion in this study.



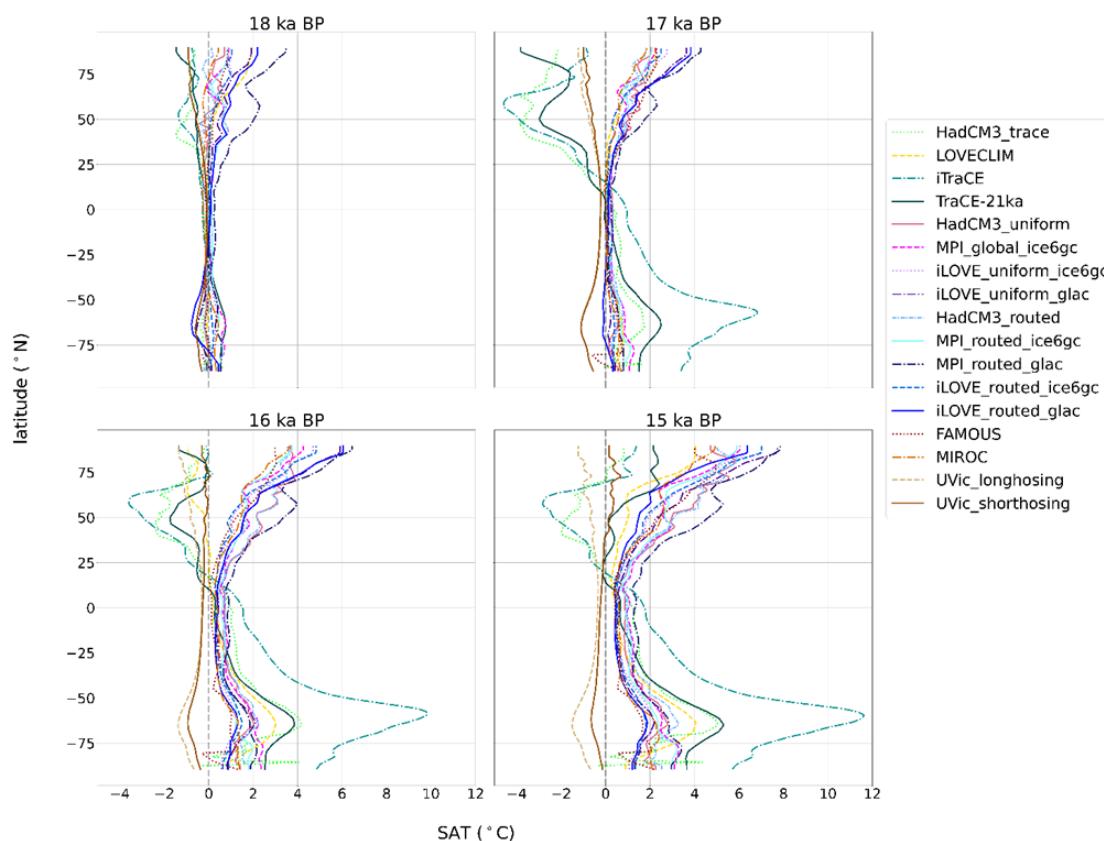
368

370 *Fig. 2: Centennial means for (a)-(d) Greenland (between 65 and 82° N and 30 and 55° W) surface air temperature anomaly*
 371 *from approximately the LGM (20 – 19.5 ka BP) for each simulation; (e)-(h) Maximum AMOC of the Northern Hemisphere at*
 372 *depth between 500 and 3500 meters. For comparison, (a)-(d) includes Greenland surface air temperature proxy record from*
 373 *Buizert et al. (2014), plotted as an anomaly from 20 ka BP in black and (e)-(h) includes the AMOC proxy $^{231}\text{Pa}/^{230}\text{Th}$*
 374 *composite record published by Ng et al. (2018) in black - note arbitrary y-axis scaling.*

374



3. Results/Discussion



376

378 *Fig. 3: Zonal average of decadal mean surface air temperature as anomalies from the LGM (20 – 19.5 ka BP) for each*
 379 *simulation. 18, 17, 16, and 15 ka BP are calculated as 60-year decadal means centred around the respective time period (e.g.,*
 380 *from 17.97 to 18.03 ka BP for 18 ka BP).*

380

381 Here, we focus on the course of the deglaciation, how it is impacted by the freshwater forcing, and
 382 how this relationship differs on a model-to-model and experimental design-to-experimental design
 383 basis. The trajectory of the AMOC in the Northern Hemisphere for each simulation follows closely the
 384 meltwater scenario chosen by the modelling group (Fig. 2). All the melt-routed, melt-uniform, and
 385 bespoke freshwater scenarios display a similar pattern throughout the deglaciation with a gradual
 386 warming of surface air temperature in the high latitudes and stronger warming compared to the
 387 TraCE-like simulations in the Northern Hemisphere (Fig. 3). The similarity between the simulations
 388 increases further into the deglaciation, with warming from the LGM in all regions by 16 ka BP for all
 389 the melt-routed, melt-uniform, and bespoke freshwater scenarios (Fig. 3 and S1). The TraCE-like
 390 simulations, however, do not follow the same trajectory, and the Northern Hemisphere, specifically



the North Atlantic, remains colder than at the LGM for most of the early deglaciation, with only
392 LOVECLIM and TraCE-21ka warming beyond the LGM in the North Atlantic by 15 ka BP (Fig. S2). This
colder region in the North Atlantic is evident in a multi-model mean of the ensemble where, on
394 average, the North Atlantic remains the coldest region throughout the early deglaciation (Fig. 4).
Around the onset of Heinrich Stadial 1 (18 ka BP), more discrepancy between simulations arises (as
396 indicated by disagreement even in the sign of change; Fig. 4) due to differences across the ensemble
in when and where the deglaciation begins as well as the freshwater fluxes applied. However, by 15
398 ka BP, at least 70% of simulations agree with the sign of the mean in most areas. More disagreement
remains in the North Atlantic, the region of highest variance across the ensemble and where the
400 different freshwater fluxes used in the simulations have the most direct impact. The ensemble-wide
consensus of a warming climate, however, is consistent with the increases in North Hemisphere
402 summer solar insolation and atmospheric CO₂ (Fig. 1a, b).

404 4.1 Timing of the deglaciation

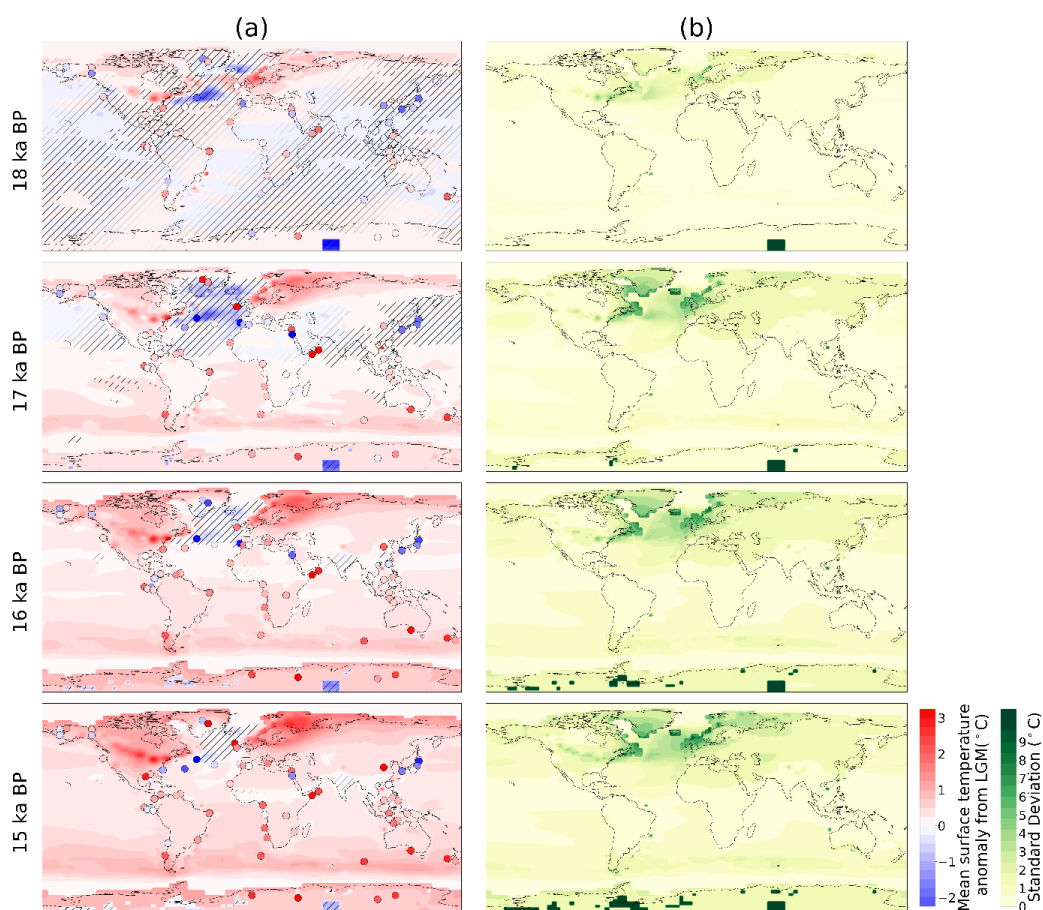
Between 20 and 15 ka BP, each of the meltwater groups, except for the *TraCE-like* simulations, have
406 relatively constant AMOC strengths. The *melt-uniform* simulations show the least millennial-scale
variability in AMOC *melt-uniform* (Fig. 2e). The *melt-routed* simulations, in comparison, have more
408 variation, aligned with the respective freshwater fluxes, and show a weakening trend starting at
~16.5 ka BP as freshwater input increases towards Meltwater Pulse 1a (Fig. 2f; Meltwater Pulse 1a
410 at 14.7 ka BP not shown). Like the *melt-routed* simulations, the *bespoke* simulations have more change
that is consistent with the freshwater flux, but for all *bespoke* simulations except for *UVic_longhosing*,
412 the AMOC strengths at 21 ka BP and at 15 ka BP are very similar.

The subset of *TraCE-like* simulations, on the other hand, show an abrupt weakening in AMOC
414 strength and an associated decrease in Greenland surface air temperature (anomaly from LGM,
calculated as anomalies from the 500-year time window from 20 – 19.5 ka BP) beginning between 18
416 and 17 ka BP depending on the simulation (Fig. 2c, g). The differences in timing of the decrease in
temperature for the *TraCE-like* simulations are likely associated with the differences in timing and
418 magnitude of the freshwater flux. For instance, *iTraCE* shows an earlier and more abrupt cooling than
TraCE-21ka. Despite both simulations reaching the same magnitude of freshwater at 17 ka BP, the
420 rate of freshwater input into the simulation between 19 ka BP and 17 ka BP differs. At 19 ka BP, there
is a larger increase in the freshwater flux in *iTraCE*, which corresponds to a smaller, but rapid decrease
422 in the AMOC strength and Greenland surface air temperature at this same time. After 19 ka BP, the
freshwater flux in *iTraCE* remains higher than in *TraCE-21ka*, and this is consistent with the sharper



424 decrease in surface air temperature in *iTraCE* in comparison to the relatively steady decrease in
425 temperature in *TraCE-21ka*.

426



428 Fig. 4: Column (a) Multi-model mean of decadal surface air temperature anomaly from the LGM (20 – 19.5 ka BP) at each
429 timestep labelled (not including the UVic simulations). Hatching denotes areas in which less than 70% of the models agree
430 with the sign of the mean. Column (b) Same as Column (a) but showing the variance. Filled circles show the proxy surface
431 temperature stack from Shakun et al. (2012) on the same colour scale. 18, 17, 16, and 15 ka BP are calculated as 60-year
432 decadal means centred around the respective time period (e.g., from 17.97 to 18.03 ka BP for 18 ka BP).

434 *HadCM3_TraCE* uses the same meltwater scenario as *TraCE-21ka*, but instead of a gradual
435 response, there is a more abrupt decrease in the Greenland surface air temperature at ~17.5 ka BP
436 and temperatures drop. The drop is as low as in *iTraCE* (with respect to the LGM) and occurs after
the freshwater flux has decreased for both *TraCE-21ka* and *HadCM3_TraCE*. Note, that *TraCE-21ka*



438 and *HadCM3_TraCE*, however, are configured with different boundary conditions (i.e., *HadCM3_TraCE*
439 uses greenhouse gas conditions on the AICC2012 timescale and the ICE-6G_C ice sheet
440 reconstruction, whereas the CCSM3 *TraCE-21ka* simulation uses ICE-5G) with the exclusion of the
441 freshwater forcing. This suggests that the freshwater forcing is a dominant driver of the abrupt
442 changes displayed in both simulations; however, the differences between them might contribute to
443 the differences in sensitivity to the meltwater flux.

444 In addition, although the meltwater scenario for *LOVECLIM* is based upon *TraCE-21ka*, the
445 freshwater flux begins later, at 17 ka BP. Presumably because of this, the decrease in surface air
446 temperature and AMOC strength is also delayed until 17 ka BP. The freshwater input is also much
447 more abrupt in comparison to *TraCE-21ka* and *iTraCE*, corresponding to the rapid transition in the
448 AMOC and surface air temperature at 17 ka BP. The implications of these differences amongst the
449 simulations in the *TraCE-like* meltwater group are further described in section 4.4.

450 The GLAC-1D ice sheet reconstruction has more variable meltwater input in comparison to
451 ICE-6G_C, at least partly due to the more frequent updates of the ice sheet geometry and associated
452 boundary conditions (every 100 years compared to every 500 years; Fig. 1c). This more variable
453 meltwater forcing presents itself in the higher variability of the AMOC strength and Greenland surface
454 air temperature (Fig. 2b, f; e.g., the sharp decline and subsequent increase in temperature and AMOC
455 strength at ~18.5 ka BP in *MPI_routed_glac* that occurs at the same time as an increase in meltwater
456 release).

457 All the simulations that do not follow the *TraCE-like* meltwater forcing follow a similar
458 trajectory throughout the deglaciation with a gradual warming of surface air temperature in
459 Greenland, except for the UVic simulations. The UVic simulations differ presumably because of the
460 *bespoke* freshwater flux that ends earlier than the end of Heinrich Stadial 1 for the short-hosed
461 simulation and after Meltwater Pulse 1a for the long-hosed simulation. The resultant impacts on the
462 dynamically simulated carbon cycle causes atmospheric CO₂ concentrations to decrease during AMOC
463 weakening, which contradicts reconstructions of this time period (e.g., Bereiter et al. 2015; Ng et al.
464 2018). Hence, in *UVic_longhosing*, decadal surface air temperature remains cold throughout the onset
465 of the deglaciation, and *UVic_shorthosing* does not begin to warm in the Northern Hemisphere until
466 the freshwater hosing is turned off at 17 ka BP (Fig. 2).

467 Across the ensemble, significant warming (defined by using a one-sided Student t-test of 99%
468 confidence with 100-year samples of surface air temperature annual means and 20 – 19.5 ka BP as
469 the LGM reference period) from the LGM occurs in most parts of the world by 18 ka BP except for in
470 the tropics where significant warming does not occur until as late as 15 – 16 ka BP (Fig. 5). The earlier



warming in the high northern latitudes is likely associated with the increase in insolation (Fig. 1a; 472 CAPE-Last Interglacial Project Members 2006; Park et al. 2019; Kapsch et al. 2021) and the impact of polar amplification; whereas the warming in the tropics is more delayed and correlates with the 474 timing of CO₂ concentration increases (Fig. 2Fig. 1b, and S3a-d). This pattern is aligned with the results from Roche et al. (2011) (see Fig. 4 by Roche et al. (2011); of which the analysis of Fig. 5 in 476 this study is based, but the LGM reference period is earlier than used here), that similarly show an earlier warming in the northern and southern high latitudes and delayed warming in the tropics. The 478 effect of the freshwater forcing on the global temperature, however, would not be incorporated in the no-melt simulations from Roche et al. (2011). Nevertheless, in the TraCE-like simulations, the 480 meltwater impact is evident by the strong cold anomalies in the North Atlantic, the region where most of the freshwater forcing is applied or drained into (Fig. 3 and 4). Warming in this region, 482 therefore, does not occur until much later in the deglaciation in comparison to the other simulations.

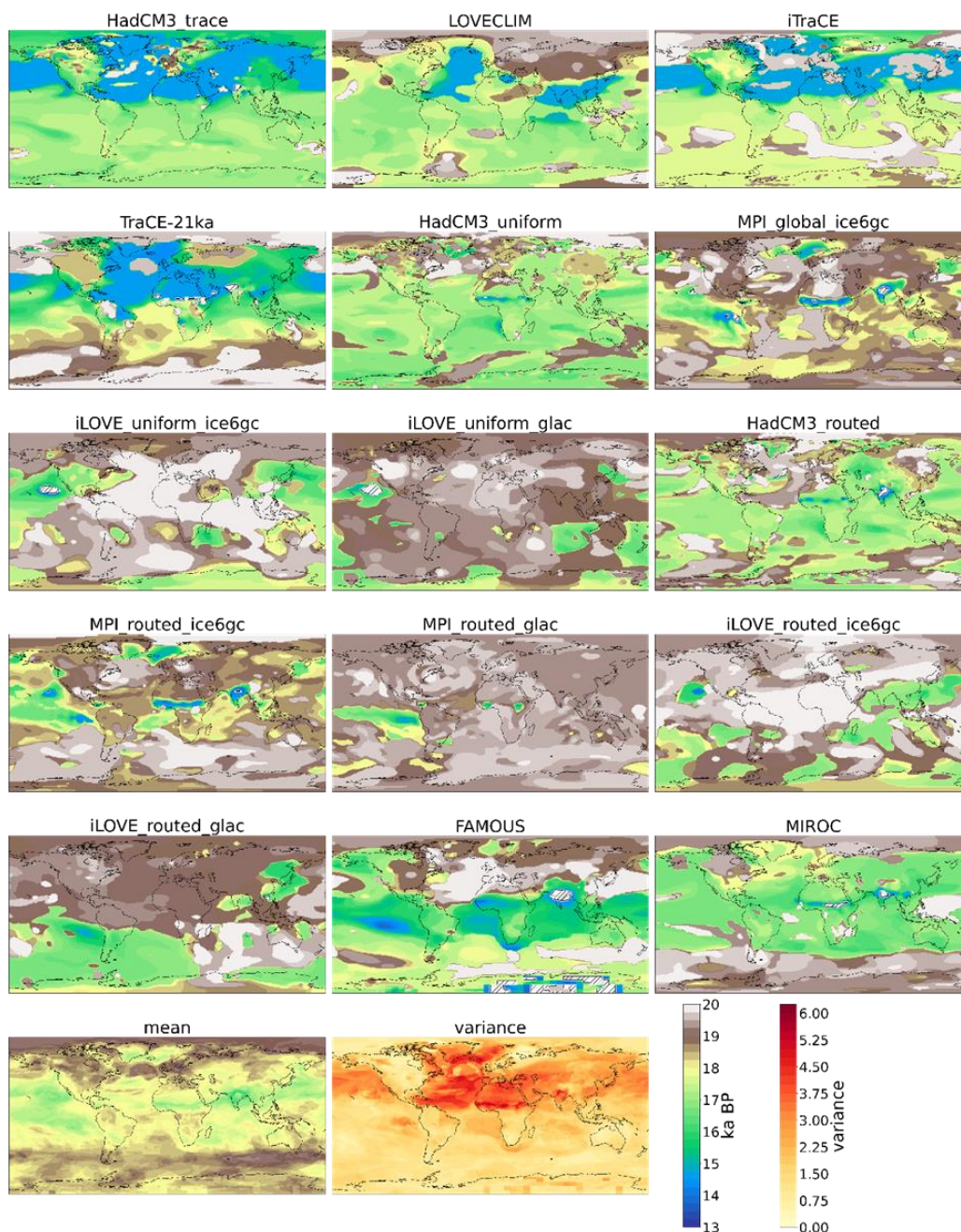
This dissimilarity in the timing of the onset of the deglacial warming is also evident in global 484 surface air temperature anomalies from the LGM (Fig. 4 and S1). Early in the deglaciation, at 18 ka BP, there is disagreement between simulations as to the timing and magnitude of the warming as well 486 as to which regions. For instance, *MPI_routed_glac* has warmed ~4 °C in the North Atlantic by 18 ka BP, whereas *MIROC* still has colder regions throughout the tropics and Pacific with respect to the LGM 488 and has only started to warm in the high latitudes, most likely associated with insolation increases (Fig. S1).

490 By 16 ka BP, all the non-*TraCE-like* simulations show consistent warming throughout the globe, whereas the *TraCE-like* simulations still have the strong cooling in the North Atlantic associated 492 with the freshwater input (Fig. 3 and S1). In the *TraCE-like* simulations (most evident in *HadCM3_TraCE* and *TraCE-21ka*), the earlier deglacial warming in the Southern Hemisphere and the 494 delayed warming in the Northern Hemisphere are due to the bipolar seesaw (Broecker 1998; Stocker 1998) associated with the simulated slowdown of AMOC within Heinrich Stadial 1 (He et al. 2013), 496 with many areas not departing from their glacial climates until after 15 ka BP (Fig. 5). This is less evident in *LOVECLIM*, potentially because the cooling from the freshwater flux occurs later, at 17 ka 498 BP, and therefore, significant warming has already occurred beforehand (as also evident by the zonal surface air temperature means; Fig. 3).

500 Unlike the other non-*TraCE-like* simulations, *FAMOUS* does not warm in the tropics until later in the deglaciation due to its late rise in atmospheric CO₂ forcing. *TraCE-21ka* similarly warms later 502 further south in the tropics, compared to *HadCM3_TraCE* and *iTraCE*, which use the AICC2012 age model for greenhouse gas forcing. The *iLOVECLIM* and *MPI* simulations, in comparison, have



504 significant warming in most areas from the immediate onset of the deglaciation. Additional
similarities are evident even amongst simulations that use the same model but different meltwater-
506 scenarios, e.g., between *HadCM3_uniform* and *HadCM3_routed* and between *MPI_routed_ice6gc* and
MPI_global_ice6gc. The HadCM3 simulations have a matching cooling region around the Labrador Sea
508 and Gulf Stream, and the MPI simulations have a matching cooling region in the Nordic Seas that each
persist until ~16 ka BP (more detail in section 4.3). UVic remains unique amongst the simulations
510 assessed in this study, because between 20 and 15 ka BP, most regions do not warm from the LGM.
The CO₂ increase begins to take precedent in *UVic_shorthosing* after 17 ka BP and the melting ice
512 sheets in North America and Fennoscandia show familiar warming patterns in the Northern
Hemisphere for ICE-6G_C: a pattern also evident in the other simulations using ICE-6G_C. This
514 warming still exists for *UVic_longhosing*, but with lower amplitude.



516

518

520

Fig. 5: Year of first significant warming from 20 ka BP, where 'significant warming' is determined using a one-sided Student *t*-test with 100-year samples of surface air temperature annual means, 99% confidence, and 20 – 19.5 ka BP as the reference period (LGM). Hatching denotes where significant warming did not occur before 13 ka BP.



522 Despite the disagreements with the timing of the deglaciation on an individual scale, the sign
of the multi-model mean of decadal surface temperature shares close agreement with the surface
524 temperature stack produced by Shakun et al. (2012), most significantly in the Southern Hemisphere
(Fig. 4). The median point-by-point difference between the multi-model mean and the proxy data is
less than 1 °C between 18 and 15 ka BP, with a median of only 0.015 °C at 18 ka BP that increases to
526 0.993 °C by 15 ka BP, indicating that the multi-model mean of the ensemble replicates the Shakun et
al. (2012) proxy stack relatively well, but that disagreement with the proxy record grows further into
528 the deglaciation. The largest discrepancies between the model output and reconstruction occur in the
North Atlantic and Greenland (after 18 ka BP), which are also areas of more disagreement across the
530 model ensemble (Fig. S4). This is the region where there are the most proxy records, and therefore
potentially the location in which the deglacial climate evolution is the best constrained (at least
532 compared to the Pacific sector, for example). The North Atlantic is also the region where most models
would show agreement for similar AMOC change, however these simulations show various AMOC
534 evolutions. The multi-model mean tends to be cooler than the proxy data in most locations, especially
the Southern Hemisphere, but is warmer in some parts of the North Atlantic, Alaska, and off the coast
536 of Japan. With much of the Northern Hemisphere too warm and Southern Hemisphere too cold, this
could argue that the representation of the bipolar seesaw is too pronounced in some simulations.
538 Interestingly, although the TraCE-like meltwater group represents the cold areas of the North Atlantic
well, those simulations have difficulty replicating the warmer core locations in this same region.
540 Conversely, the other meltwater groups present the opposite difficulty—they are better at replicating
the warmer regions of the North Atlantic while failing to represent the cold ones (not shown). This
542 suggests the potential need for subsequent investigations of broader model structure and how we
interpret reconstructions (i.e., specific data points).

544

4.2 Linking surface climate, ocean circulation, and greenhouse gas forcing

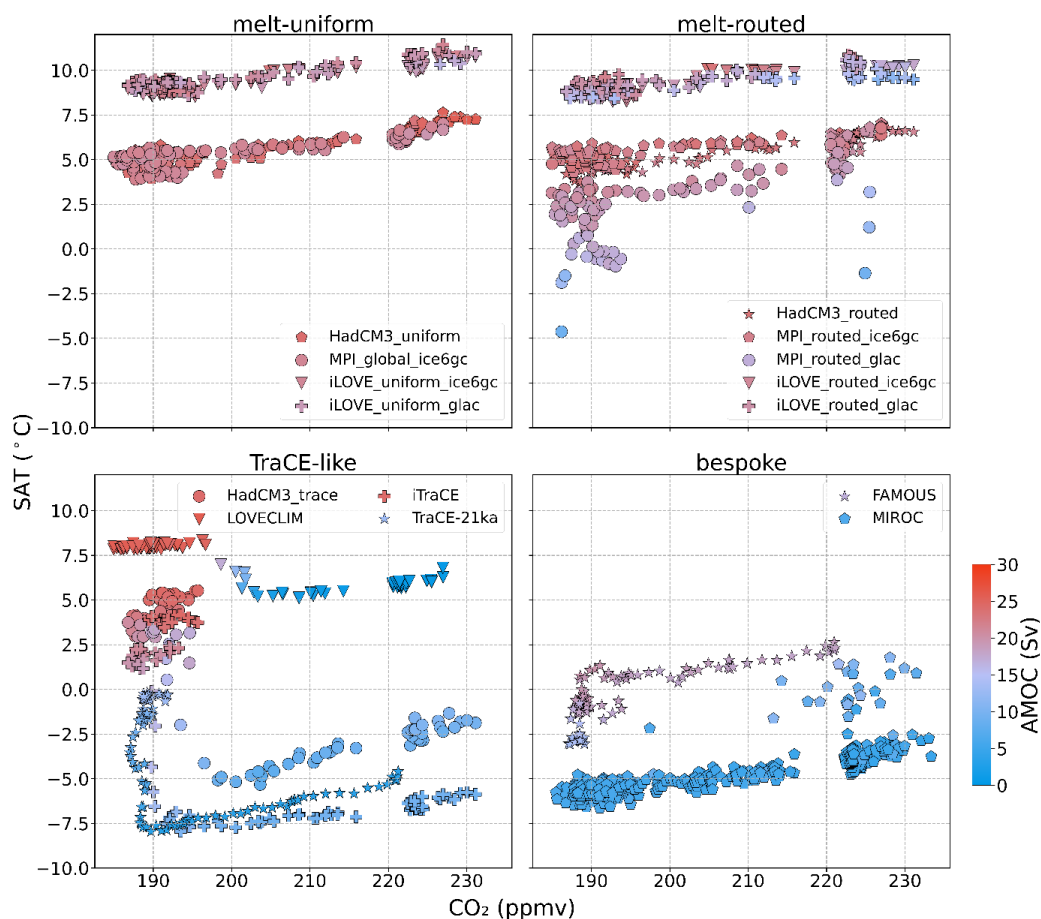
546 In every simulation, there is the expected interrelation between surface air temperature in the North
Atlantic, CO₂ concentration, and AMOC. As CO₂ increases, surface air temperature increases, as
548 demonstrated by the increasing trends on each panel of Fig. 6 surface air temperature is higher when
the AMOC is stronger, clearly shown by *LOVECLIM*. This relationship is illustrated further by the R²
550 values determined by a linear regression model across the entire period between 20 and 15 ka BP on
a decadal temporal scale (Fig. 7 Fig. 8). The results from the linear regression show that during the
552 period of 20 to 15 ka BP, surface air temperature in the *TraCE-like* simulations has a stronger positive
correlation with AMOC, and the other simulations in the ensemble have a stronger positive



554 correlation with CO₂. For instance, the *TraCE-like* simulations have higher R² values in the North
Atlantic than the other meltwater groups, presumably because changes between AMOC and surface
556 air temperature correspond in the *TraCE-like* simulations between 20 and 15 ka BP, whereas the other
simulations have a stable ocean circulation and very little temperature change during this time period
558 (Fig. 2). FAMOUS, which has a stronger freshwater forcing between 20 and 15 ka BP in comparison
to the other non-*TraCE-like* simulations, also has higher R² values in the North Atlantic region, though
560 dampened relative to that of the *TraCE-like* simulation. The simulations with little AMOC and surface
air temperature change show very low correlations between the two variables throughout the globe
562 (e.g., iLOVECLIM simulations, the ICE-6G_C MPI simulations, and MIROC). However, the *melt-routed*
GLAC-1D simulations, in comparison to their ICE-6G_C same-model counterparts, exhibit higher
564 correlations, especially in the case of *MPI_routed_glac*.

The positive slope in the North Atlantic region for the *TraCE-like* simulations demonstrates
566 the positive correlation between AMOC and surface air temperature changes, whereas the rest of the
globe has a more negative correlation in most simulations, regardless of their meltwater group. This
568 relationship is representative of the bipolar seesaw. The *TraCE-21ka* simulation most clearly exhibits
this bipolar connection between the Northern and Southern Hemispheres with a strong positive
570 correlation between AMOC and surface air temperature in the North Atlantic and a strong negative
correlation in the Southern Ocean.

572



574 Fig. 6: Absolute surface air temperature over the North Atlantic (between 35 and 60° N and -60 and 0° E) as a function of CO₂
 576 concentration with symbols' shading representing the strength of the AMOC (Sv) split into groups defined by meltwater
 578 scenario. 50-year means are shown for each simulation except for MIROC, for which decadal means are shown to capture its
 temporally finer-scale variability. See Fig. S5 for the same analysis displayed as anomalies from 20 ka BP.

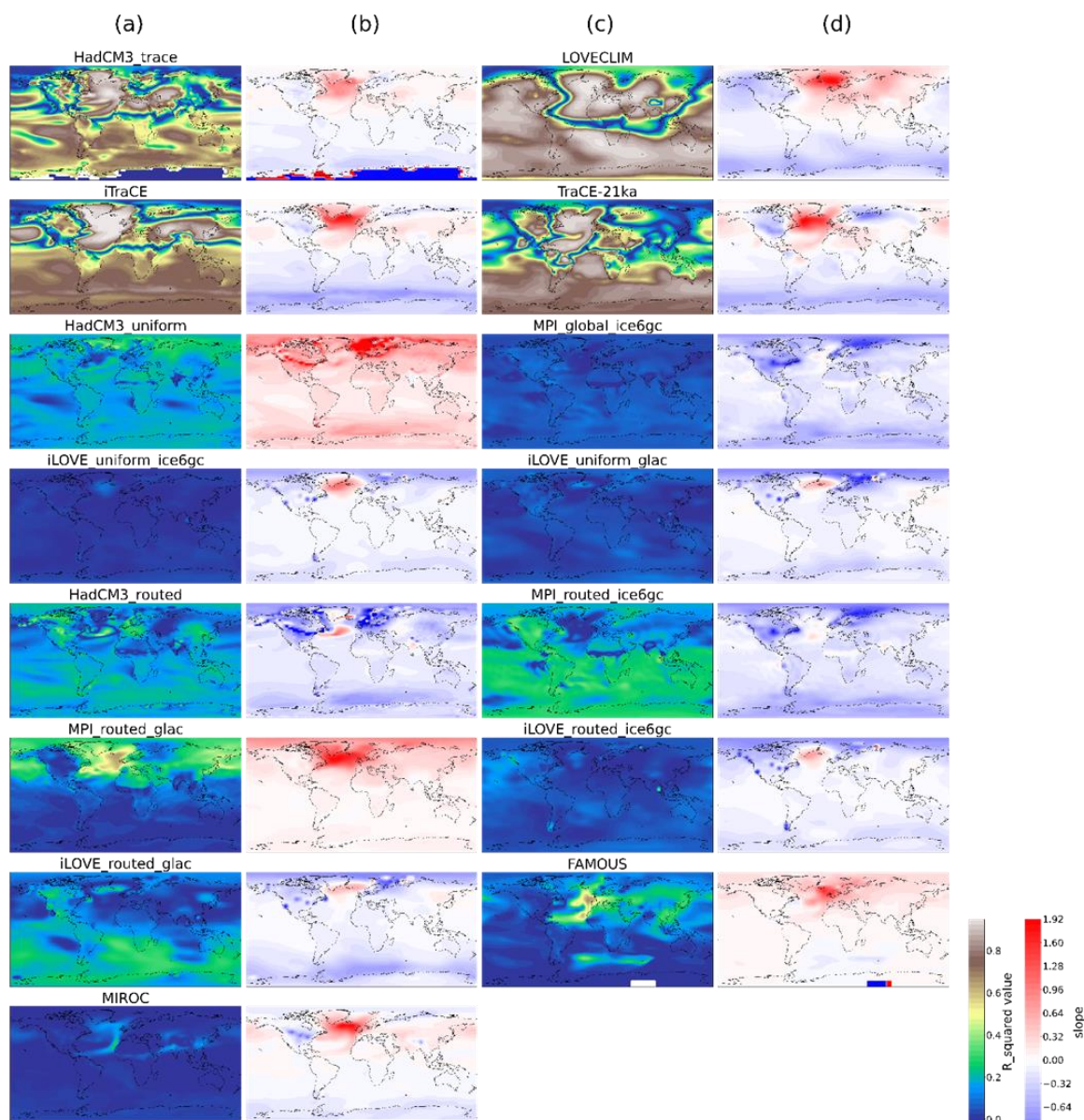
578

The relationship between CO₂ and surface air temperature (Fig. 8) in the Northern
 580 Hemisphere is nearly opposite to the relationship between AMOC strength and surface air
 582 temperature for *HadCM3_TraCE*, *iTraCE*, and *TraCE-21ka*, with the areas of strong and positive
 584 correlation between AMOC and surface air temperature showing weaker and negative correlation
 586 between CO₂ and surface air temperature. This suggests that in the early deglaciation, if the AMOC is
 weakening/already weak because of the freshwater forcing when CO₂ starts to rise, the impact of CO₂
 might be dampened or postponed in the Northern Hemisphere, whereas a strong correlation with
 surface air temperature remains in the Southern Hemisphere. The results by Sun et al. (2022) show

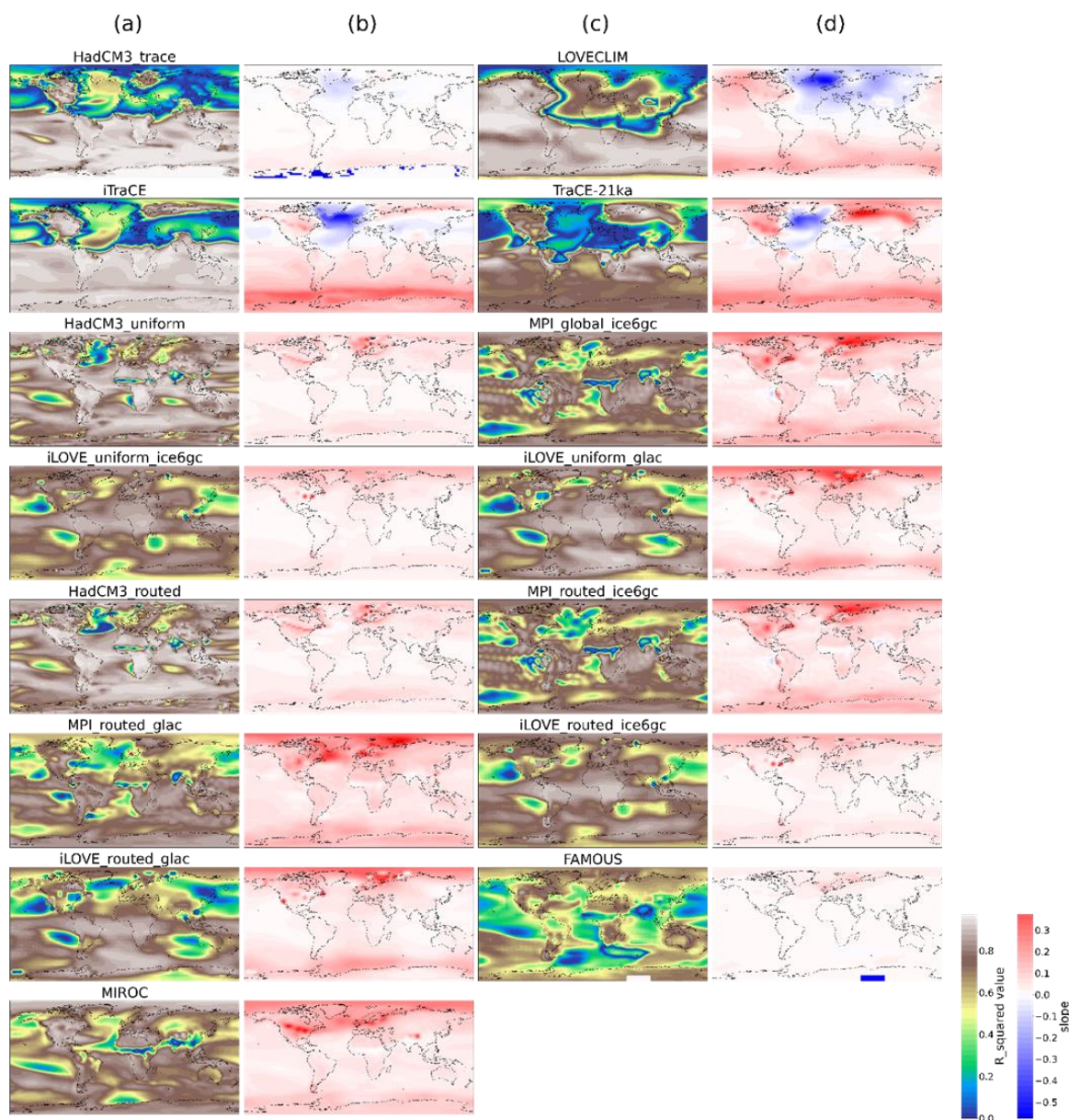


that the CO₂ increase could assist with the later transition out the weak AMOC state and into the
588 Bølling Warming (not shown here). Unlike the other simulations in the *TraCE-like* meltwater group,
the strength of correlation between AMOC and surface air temperature versus with CO₂ does not
590 change for *LOVECLIM*, potentially because the AMOC weakening and the CO₂ increase are concurrent.
The simulations with weaker correlation between CO₂ and surface air temperature in regions of the
592 tropics (e.g., *FAMOUS* and parts of Sub-Saharan Africa in *MIROC*, *MPI_global_ice6gc*, and
HadCM3_routed) also display delayed warming in these same locations (Fig. 5). Increases in obliquity
594 are shown to delay warming in the tropics, specifically in these same parts of Africa as well as India,
potentially due to increased cloud coverage and therefore cooling (Erb et al. 2013). In addition, the
596 lag between the start of the CO₂ concentration increase (~18 ka BP or later depending on the
timescale used) and the insolation increase (~20 ka BP) can disrupt the correlation between CO₂ and
598 surface air temperature and create a localised delay in warming of the tropics (as also demonstrated
in Fig. 5). Note that the analysis in Figures 7 and 8 only goes until 15 ka BP whereas the analysis in
600 Fig. 5 reaches until 13 ka BP. The simulations with the very weak correlations between AMOC
and surface air temperature (*iLOVECLIM*, MPI simulations, and *MIROC*) demonstrate globally high
602 correlations with CO₂ except for a few concentrated regions. These regions of lower correlation are
similar between simulations run by the same model and could indicate changes in upwelling strength
604 during this time period.

It is important to note, however, that during the chosen time period, only the *TraCE-like*
606 simulations have strong and corresponding changes in the AMOC and surface air temperature. The
suggested relationships could be checked by continuing this study through the later parts of the
608 deglaciation to encompass greater amplitudes of change in the non-*TraCE-like* simulations.



610 Fig. 7: Spatial correlation of AMOC strength and surface air temperature using a linear regression model for the time period
 20 - 15 ka BP using decadal means. Columns (a) and (c): R^2 values as a result of the linear regression. Columns (b) and (d):
 612 corresponding slopes to simulation in Column (a) or (c) as a result of the linear regression.



614

616

618

Fig. 8: Spatial correlation of CO₂ concentration and surface air temperature using a linear regression model for the time period 20 - 15 ka BP using decadal means. Columns (a) and (c): R² values as a result of the linear regression. Columns (b) and (d): corresponding slopes to simulation in Column (a) or (c) as a result of the linear regression.



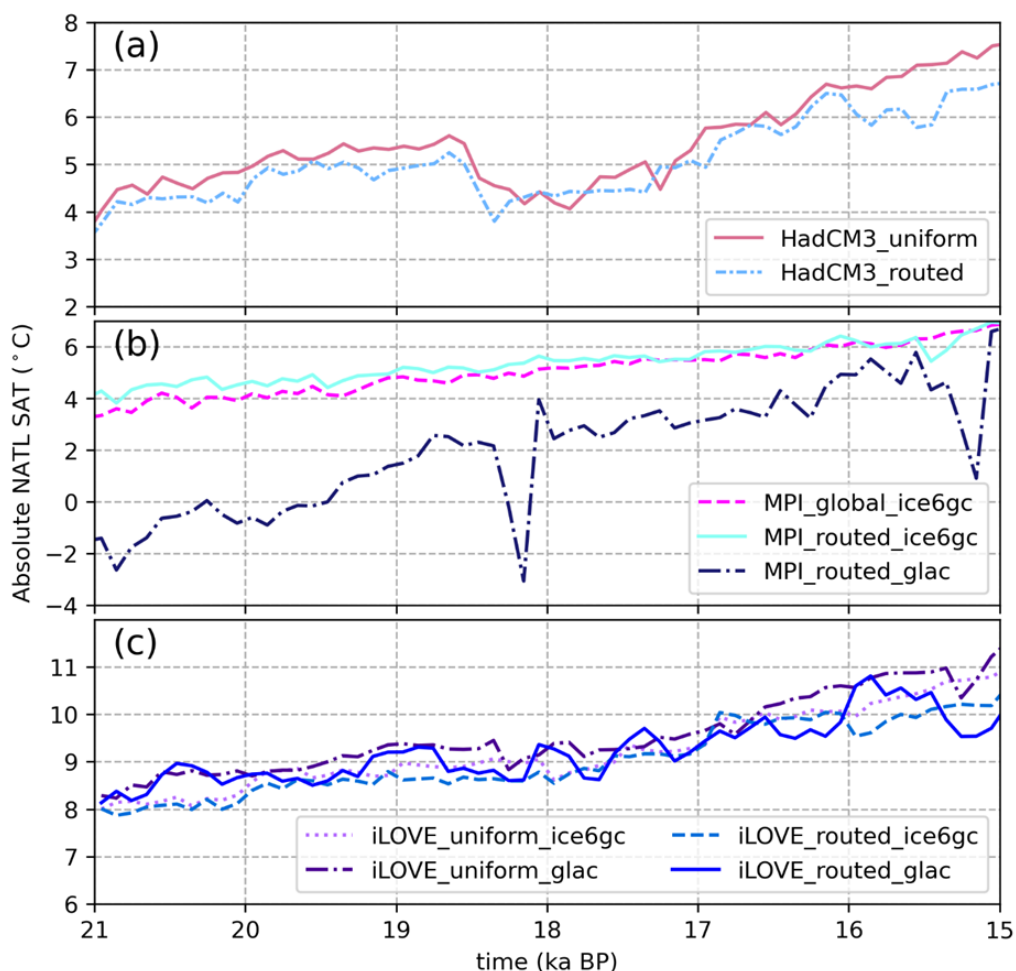
4.3 Impact of different climate forcings on model output

620 In this study, we have included multiple simulations from the HadCM3, MPI, and iLOVECLIM
622 modelling groups. These three modelling groups tested different PMIP4 boundary condition/forcing
options: for example, implementing the *melt-routed* or *melt-uniform* scenario for the same ice sheet
and/or using different ice sheets and associated meltwater scenarios (Table 1). Experimenting with
624 the range of options the PMIP4 protocol enables us to review the impact of different climate forcings
on the resultant model output.

626 The AMOC for each of the HadCM3, MPI, and iLOVECLIM simulations is impacted by the
chosen meltwater scenario during the deglaciation (see section 4.1); however, between 21 and 15 ka
628 BP, the differences between the AMOC trajectory appear to be less affected by the meltwater scenario
and instead more significantly affected by the choice of ice sheet reconstruction (Fig. 9). For instance,
630 when we compare the simulations with the different meltwater scenarios, but with the same ice sheet
reconstruction (e.g., ICE-6G_C), i.e., *HadCM3_uniform* and *HadCM3_routed*, *iLOVE_uniform_ice6gc* and
632 *iLOVE_routed_ice6gc*, and *MPI_global_ice6gc* and *MPI_routed_ice6gc*, we notice multiple similarities
between the deglaciation trajectory, spatially and temporally. For instance, the HadCM3 simulations
634 begin at a very similar surface air temperature in the North Atlantic at the start of the deglaciation
(~4 °C at 21 ka BP) and follow a comparable warming trajectory until 15 ka BP (reaching ~7 °C; Fig.
636 9) despite the application of different meltwater scenarios, though the *melt-routed* simulation does
remain colder in the North Atlantic than the *melt-uniform* simulation throughout the time period. In
638 addition, spatially, as anomalies from the LGM (Fig. 3 and S1), the simulations look almost
indistinguishable. Both display surface air temperature cooling along the Gulf Stream, and warming
640 in locations of ice sheet melt, such as the Eurasian ice sheet in Fennoscandia and at the edge of the
Laurentide ice sheet in North America. The most evident difference between the simulations is that
642 *HadCM3_uniform* is colder than *HadCM3_routed* in the Labrador Sea and warmer in the Norwegian
Seas, corresponding with differences in sea ice concentration—*HadCM3_uniform* has a higher sea ice
644 concentration in the Labrador Sea than *HadCM3_routed* and a lower concentration in the Norwegian
Seas (Fig. S6A and B). This pattern also corresponds to the dissimilarities in the convection sites
646 between the two simulations as the *melt-uniform* simulation has more convection further south, along
the sea ice edge, and in the Norwegian Seas, whereas the mixed-layer depth in the *melt-routed*
648 simulation is deeper in the Labrador Sea (Fig. S6C). *HadCM3_TraCE* has the same dipole pattern as
the other HadCM3 simulations, with cooling along the Gulf Stream and into Greenland and the
650 Labrador Sea, and warming over Fennoscandia; however, this signal is weak compared to the strong
cooling in the North Atlantic due to the larger freshwater forcing applied.



652



654 Fig. 9: Absolute surface air temperature in the North Atlantic (between 35 and 60° N and -60 and 0° E) for the HadCM3, MPI-
 656 ESM, and iLOVECLIM simulations. Note: to capture variability, y-axis limits are not the same for each panel. Absolute surface
 air temperature in the North Atlantic for the entire ensemble is shown in Fig. S3e – h.

658 Likewise, *MPI_global_ice6gc* and *MPI_routed_ice6gc* both begin at ~4 °C at the start of the
 deglaciation in the North Atlantic and then warm at a comparable rate, but slower than the HadCM3
 660 simulations, warming ~3 °C by 15 ka BP rather than ~5 °C. The MPI simulations, like the HadCM3
 simulations, also share a similar spatial pattern with an area of strong cooling in the Nordic Seas and
 662 stronger warm patches off the coast of north-western North America and in the North Sea (Fig. S1).
 This pattern appears to be independent of the ice sheet reconstruction, because *MPI_routed_glac* has
 664 the same areas of relative cold and warmth at 18 ka BP, but the signal is weaker, likely because



MPI_routed_glac is ~ 5 °C warmer in the North Atlantic at the start of the deglaciation than the ICE-6G_C simulations. Temporally, however, *MPI_routed_glac* displays more surface air temperature variability in the North Atlantic with abrupt climate changes as large as 5 °C and AMOC decreases of ~ 9 Sv at ~ 18.2 and 15.2 ka BP, most likely following the higher-frequency variability in the meltwater input from the GLAC-1D ice sheet reconstruction (Fig. 2Fig. 6), but also because *MPI_routed_glac* is significantly colder at the LGM compared to its ICE-6G_C counterparts. Kapsch et al. (2022) show that the MPI simulations that are colder during the LGM lie closer to a critical threshold of AMOC variability. This aligns with the findings of Oka et al. (2012) and Klockmann et al. (2018) that demonstrate that the AMOC becomes more sensitive to perturbations, such as ice sheet topography, and the resultant wind stress, and CO₂ concentrations, when it is closer to an existing temperature threshold. Ensemble absolute surface air temperatures in the North Atlantic (Fig. S3e-h) show that multiple simulations in the ensemble are colder than *MPI_routed_glac* at the LGM, but only *MIROC's* AMOC appears to be close to a critical threshold of variability, as indicated by the changes in maximum AMOC strength towards 15 ka BP.

iLOVE_routed_glac has a similar, but less pronounced, variability of the AMOC and corresponding decreases in Greenland surface air temperature to *MPI_routed_glac* (Fig. 2b). However, in the North Atlantic, neither the *iLOVE_routed_glac* simulation nor *iLOVE_uniform_glac* exhibit significantly more variability than the ICE-6G_C *iLOVECLIM* simulations (relative to *MPI_routed_glac* and its ICE-6G_C counterparts). Spatially, the ICE-6G_C and GLAC-1D simulations are also nearly indiscernible (Fig. S1), except at the beginning of the deglaciation in the Southern Hemisphere, where surface air temperatures remain cooler for longer in the GLAC-1D simulations. This suggests that *iLOVECLIM* is less sensitive to freshwater perturbations than MPI-ESM-CR under these background conditions; however, this depends on how both modelling groups calculate their freshwater flux, which can vary, technically, even though the same ice sheet reconstruction is used (see section 3), as well as, and potentially more importantly, the fact that these simulations are performed with two very different models. For example, *iLOVECLIM* is an Earth system model of intermediate complexity (EMIC) with three atmospheric layers (see Table 1), whereas MPI-ESM-CR is an Earth system model (ESM) with 31 atmospheric levels, and thus can represent topographic feedbacks on the atmosphere with higher complexity and at finer-scale resolution. Unfortunately, more simulations using a GLAC-1D derived freshwater flux do not exist to compare to *MPI_routed_glac* and *iLOVE_routed_glac* and to get more robust results. Further simulations from other model types using both ice sheet reconstructions would be beneficial to understanding whether the systematic differences between the models are contributing to the differences in sensitivity to the freshwater forcing.



698 4.4 Sensitivity of climate models to similar forcing(s)

700 All simulations, with the exclusion of the UVic simulations, *TraCE-21ka*, and *FAMOUS*, use the
greenhouse gas forcing on the AICC20212 timescale, with an increase in atmospheric CO₂
702 concentration at ~17.5 ka BP. In contrast, in *TraCE-21ka* and *FAMOUS*, the CO₂ concentration does not
begin increasing until ~17 ka BP. This delayed increase in CO₂ postpones the warming of the
deglaciation in these simulations, as is evident in the tropical regions (Fig. 3Fig. 5, and S3). *MIROC*,
704 despite not having a delayed CO₂ increase, also displays delayed warming in the tropics, like that of
FAMOUS. This could be due to the stronger impact of the orbital forcing in *MIROC* taking precedent
706 over the CO₂ forcing earlier in the deglaciation (Obase and Abe-Ouchi 2019).

Contrasting sensitivities of the models used for the *TraCE-like* simulations is evident in the
708 response of the AMOC to the freshwater forcing and corresponding changes in Greenland surface air
temperature in the different models (Fig. 2). By 17 ka BP, all four simulations have reached a similar
and constant freshwater flux (with *iTraCE* ~0.05 Sv, or 33%, higher). The four simulations, however,
begin with a range of different AMOC strengths. *LOVECLIM* has the strongest LGM AMOC at ~28 Sv,
712 *TraCE-21ka* with the weakest LGM AMOC at ~12 Sv, and *HadCM3_TraCE* and *iTraCE* are in the middle
of the cluster, starting with an AMOC strength of ~24 Sv (see Table S1; Fig. 2g). Note that
714 *HadCM3_TraCE* and *iTraCE* start at 20 ka BP, whereas *LOVECLIM* and *TraCE-21ka* start at 21 and 22
ka BP respectively.

716 Despite beginning the deglaciation with the strongest AMOC, *LOVECLIM*'s ocean circulation is
also the most sensitive to the freshwater perturbation, causing its AMOC to crash to the weakest
718 AMOC state of all the simulations (Fig. 2g). The temperature change in the *LOVECLIM* simulation,
however, is comparable to the temperature change in *TraCE-21ka* despite the very different AMOC
720 responses to the freshwater forcing. The AMOC collapses to nearly 0 Sv, but Greenland surface air
temperature only decreases by ~5 °C.

722 The Greenland surface air temperature response in *HadCM3_TraCE* and *iTraCE* appears to be
impacted similarly by the change in AMOC strength, with both simulations following comparable
724 trajectories throughout the deglaciation despite *iTraCE* having a larger freshwater flux. Both
simulations exhibit an AMOC decrease of ~14 Sv and ~ -7 °C of temperature change between 19 and
726 16 ka BP. In addition, although *TraCE-21ka* and *HadCM3_TraCE* use the exact same freshwater flux,
the *HadCM3_TraCE* simulation exhibits a decrease in AMOC strength of over ~14 Sv and a
728 corresponding decrease in surface air temperature of ~10 °C in Greenland, whereas *TraCE-21ka*'s
AMOC strength weakens by only ~9 Sv and Greenland surface air temperature only decreases by ~4
730 °C. This suggests that the *HadCM3* simulation is more sensitive to freshwater perturbations than



TraCE-21ka, but also that under the simulated climate conditions, Greenland surface air temperature
732 in HadCM3 is also more sensitive to corresponding AMOC changes compared to the other models.
Additional exploration would be interesting to determine what different aspects between
734 *HadCM3_TraCE* and *TraCE-21ka* could be contributing to the discrepancies in sensitivity (e.g.,
whether it could be the initial conditions, other boundary conditions, parameter choices, or simply
736 model structure). The lower sensitivity of CCSM3 to freshwater perturbations is further investigated
by He and Clark (2022) by rerunning *TraCE-21ka* but with no freshwater input during the Holocene.
738 This version of the simulation is in better agreement with proxy Holocene AMOC kinematic
reconstructions (McManus et al. 2004; Lippold et al. 2019).

740 The differences in model sensitivity are less observable in the simulations that apply
meltwater forcing in accordance with the PMIP4 protocol's ice sheet consistent recommendations, as
742 discussed in section 4.3.

744 *4.5 Meltwater paradox*

There has been ongoing debate on how much meltwater to input into simulations of the last
746 deglaciation, and these results highlight the impact of the decision. The debate has stemmed from a
so called 'meltwater paradox' that exists between the choice of large and geologically- inconsistent
748 meltwater forcings that successfully produce abrupt climate events versus glaciologically realistic
meltwater fluxes that do not. This paradox is particularly evident in the last deglaciation during
750 Heinrich Stadial 1 and the Bølling Warming. Heinrich Stadial 1, for instance, is associated with weak
ocean circulation strength (Lynch-Stieglitz 2017; Ng et al. 2018; Pöppelmeier et al. 2023a) and cold
752 climate conditions in multiple regions. There has been difficulty reconciling a weak AMOC concurrent
with a small amount of 'realistic' freshwater release, as determined by the ice sheet reconstructions,
754 in model simulations of the early deglaciation. Because of this, some model experiments (e.g.,
simulations in the *TraCE-like* meltwater group) have required, by design, overly-large quantities of
756 freshwater forcing to collapse their initially strong AMOCs and produce an abrupt cooling event like
that of the surface air temperature proxy records of the Hulu and Kulishu Caves (Wang et al. 2001;
758 Ma et al. 2012). Ivanovic et al. (2018) suggested that the AMOC weakening targeted in these
simulations is too large, and that a smaller meltwater flux inducing more modest North Atlantic
760 change may be sufficient to drive the recorded Heinrich Stadial climate. However, fully transient
simulations that include only meltwater that is consistent with the ice sheet reconstructions (i.e.,
762 *HadCM3_routed*, *MPI_routed_ice6gc*, *MPI_routed_glac*, *iLOVE_routed_ice6gc*, *iLOVE_routed_glac*, and



764 their corresponding *melt-uniform* simulations), do not achieve either the AMOC change nor the surface climate signal of the Heinrich Stadial.

766 In this context, the MIROC last deglaciation simulation, is unique because it simulates the weak AMOC and cold surface air temperatures of Heinrich Stadial 1 (Fig. 2h and S3h) and the resumption of the AMOC of the Bølling Warming without releasing an unrealistically large amount of
768 freshwater (not shown as this paper only covers until 15 ka BP; see Obase and Abe-Ouchi 2019). Instead, a cold, weak-AMOC state is achieved with a gradually increasing meltwater flux that remains
770 below the ice volume loss in the reconstruction. Notably, however, this simulation uses the *increasing* meltwater flux to regulate the timing of the abrupt resumption of the AMOC and therefore, displays a
772 different sensitivity to freshwater input compared to the rest of the last deglaciation ensemble. This is likely in part due to the very weak LGM AMOC state at the start of the simulation, which also plays
774 a role in the surface air temperature response and may make the simulation more susceptible to a small freshwater flux. As the insolation and CO₂ concentrations increase, *MIROC's* AMOC begins to
776 become unstable, and with the meltwater input into the North Atlantic gradually rising, it is eventually pushed to a point where the AMOC suddenly strengthens at ~14.7 ka BP (Obase and Abe-
778 Ouchi, 2019; the precise timing of AMOC recovery depends on the meltwater forcing). The AMOC and Greenland surface air temperature abruptly increase whilst the meltwater flux in the North Atlantic
780 is maintained. As the only PMIP4 last deglaciation simulation (LDv1 or previous) to simulate a weak ocean circulation at the onset of the deglaciation and then its later rapid resumption *even* with a
782 continuous freshwater flux, this simulation may offer important insight to the conditions under which abrupt deglacial climate change may occur. Nonetheless, even this model cannot reproduce the
784 Heinrich Stadial-Bølling Warming transition under Meltwater Pulse 1a-like freshwater forcing. Thus, the meltwater paradox of the last deglaciation remains.

786 4. Conclusion

This study presents results from 17 simulations of the early part of the last deglaciation (20-15 ka BP) performed with nine different climate models. Our analyses show the first assessment of these
788 simulations and display the similarities and differences between the model results as shown through the timing of the deglaciation, spatial and temporal surface air temperature changes, the link between
790 the surface climate, ocean circulation, and CO₂ forcing, and how the different models respond to different forcings. The impact of the chosen meltwater scenario on the model output has defined every result of this multi-model intercomparison study. The course of the deglaciation is consistent
792 between simulations except when the freshwater forcing is above 0.1 Sv—at least 70% of the
794



796 simulations agree that there is warming by 15 ka BP everywhere excluding the location of meltwater
input. However, for simulations with freshwater forcings that exceed 0.1 Sv from 18 ka BP, warming
is delayed in the North Atlantic and surface air temperature correlations with AMOC strength are
798 much higher. The resultant impacts of CO₂ forcing and increasing insolation (i.e., ice sheet melt and
surface temperature warming) are reduced by the large freshwater fluxes imposed, delaying the
800 warming in the Northern Hemisphere for these simulations. Nonetheless, the average of the ensemble
displays the high latitudes beginning to deglciate first in response to insolation and polar
802 amplification and later warming occurring in the tropics in correlation with the rising CO₂ trajectory.
The timing of the rise in CO₂ concentration differs between simulations depending on timescale of
804 the CO₂ reconstruction, delaying warming further in the tropics for simulations with a later CO₂
increase.

806 Simulations run by the same model (such as those from HadCM3, MPI-ESM, and iLOVECLIM)
show comparable surface climate patterns despite the use of a different ice sheet reconstruction or
808 the *melt-routed* versus *melt-uniform* freshwater scenarios. The main differences noted during this
time period include slower warming in the North Atlantic in the *melt-routed* simulations, additional
810 temporal variability in the GLAC-1D simulations, and faster warming in the GLAC-1D simulations.
Simulations run with different models, but similar boundary conditions, provide insight into the
812 sensitivity of the model to a particular forcing. We suggest that LOVECLIM's AMOC is the most
sensitive to freshwater perturbation and CCSM3's is the least sensitive; although, this is not
814 necessarily consistent with the sensitivity of the corresponding surface air temperature changes
because of complexity in how surface air temperature is linked to AMOC and other transient climate
816 forcings.

This multi-model intercomparison project has been beneficial to compare simulations of different
818 forcings to represent some of the uncertainty of the time period; however, it has also posed the
challenge of drawing direct model-to-model conclusions. It would be ideal to be able to compare more
820 simulations with the same experimental design to learn more about model sensitivities and test
additional plausible scenarios of climate changes during the last deglaciation. Hence, this study may
822 guide the design of future protocols for multi-model comparisons of the last deglaciation. One of these
protocols could also assist with narrowing down the uncertainties regarding the meltwater paradox;
824 for instance, the simulations that follow the *TraCE-like* meltwater scenario display larger variability
in the AMOC and Greenland surface air temperature, following more closely with proxy records of the
826 respective variables. However, to achieve this, the *TraCE-like* meltwater scenarios include freshwater
fluxes that are much larger than the amount deemed 'realistic' by the ice volume change in ice sheet



828 reconstructions of the time period. In contrast, simulations that follow the ice sheet reconstruction,
show less agreement with the AMOC and Greenland surface air temperature proxy records, but show
830 a more gradual warming throughout the deglaciation that has more agreement with surface
temperature proxy records, globally. Because meltwater input that is not realistic has such a large
832 impact on the results—dominating over other deglacial forcings, there is difficulty comparing
simulations that do and do not choose this *TraCE-like* scenario. Thus, additional experiments with an
834 ensemble of models testing out the meltwater scenario options could assist with unravelling the
current meltwater paradox.

836 5. Code availability

Python code will be posted on a Git Hub repository called '*pmip_ldv1_analysis_snoll*'.

838 6. Data availability

Data will be available through a University of Leeds DOI that is currently being set up.

840 7. Author contribution

The study conception was developed by the PMIP4 Working Group, consisting of RI, LM, TO, AA, NB,
842 MK, UM, and PV. BS, LG, SS, and RI contributed to the study design, with LM, TO, and AA providing
additional feedback and close communication with BS. The design of the experiments and running
844 of them was performed by RI, LG, LM, TO, AA, NB, CH, FH, MK, UM, JM, and PV. Material preparation
and data collection was performed by BS. The manuscript was prepared by BS with contributions
846 from all co-authors, who read and approved the final manuscript.

8. Competing interests

848 LM is a member of the editorial board of *Climate of the Past*, but otherwise the authors declare that
they have no conflict of interest. The authors consent to participation and publication.

850 9. Funding

BS is supported by the Leeds-York-Hull Natural Environment Research Council (NERC) Doctoral
852 Training Partnership (DTP) Panorama under grant NE/S007458/1.

10. References

- 854 Alley RB (2000) The Younger Dryas cold interval as viewed from central Greenland. *Quaternary
Science Reviews* 19:213–226. [https://doi.org/10.1016/S0277-3791\(99\)00062-1](https://doi.org/10.1016/S0277-3791(99)00062-1)
- 856 Argus DF, Peltier WR, Drummond R, Moore AW (2014) The Antarctica component of postglacial
rebound model ICE-6G_C (VM5a) based on GPS positioning, exposure age dating of ice



- 858 thicknesses, and relative sea level histories. *Geophysical Journal International* 198:537–563.
<https://doi.org/10.1093/gji/ggu140>
- 860 Armstrong E, Izumi K, Valdes P (2022) Identifying the mechanisms of DO-scale oscillations in a
862 GCM: a salt oscillator triggered by the Laurentide ice sheet. *Clim Dyn*.
<https://doi.org/10.1007/s00382-022-06564-y>
- 864 Bereiter B, Eggleston S, Schmitt J, et al (2015) Revision of the EPICA Dome C CO₂ record from 800
to 600 kyr before present: Analytical bias in the EDC CO₂ record. *Geophys Res Lett* 42:542–
549. <https://doi.org/10.1002/2014GL061957>
- 866 Berger AndréL (1978) Long-Term Variations of Daily Insolation and Quaternary Climatic Changes. *J*
868 *Atmos Sci* 35:2362–2367. [https://doi.org/10.1175/1520-0469\(1978\)035<2362:LTVODI>2.0.CO;2](https://doi.org/10.1175/1520-0469(1978)035<2362:LTVODI>2.0.CO;2)
- 870 Bitz CM, Chiang JCH, Cheng W, Barsugli JJ (2007) Rates of thermohaline recovery from freshwater
pulses in modern, Last Glacial Maximum, and greenhouse warming climates. *Geophys Res*
Lett 34:L07708. <https://doi.org/10.1029/2006GL029237>
- 872 Böhm E, Lippold J, Gutjahr M, et al (2015) Strong and deep Atlantic meridional overturning
874 circulation during the last glacial cycle. *Nature* 517:73–76.
<https://doi.org/10.1038/nature14059>
- 876 Bouttes N, Lhardy F, Quiquet A, et al (2023) Deglacial climate changes as forced by different ice
sheet reconstructions. *Clim Past* 19:1027–1042. <https://doi.org/10.5194/cp-19-1027-2023>
- 878 Bouttes N, Lhardy F, Quiquet A, et al (2022) Deglacial climate changes as forced by ice sheet
reconstructions. *Climate Modelling/Modelling only/Milankovitch*
- 880 Braconnot P, Harrison SP, Kageyama M, et al (2012) Evaluation of climate models using
palaeoclimatic data. *Nature Clim Change* 2:417–424.
<https://doi.org/10.1038/nclimate1456>
- 882 Braconnot P, Otto-Bliesner B, Harrison S, et al (2007) Results of PMIP2 coupled simulations of the
884 Mid-Holocene and Last Glacial Maximum – Part 1: experiments and large-scale features.
Clim Past 3:261–277. <https://doi.org/10.5194/cp-3-261-2007>
- 886 Bradtmiller LI, McManus JF, Robinson LF (2014) 231Pa/230Th evidence for a weakened but
persistent Atlantic meridional overturning circulation during Heinrich Stadial 1. *Nat*
Commun 5:5817. <https://doi.org/10.1038/ncomms6817>
- 888 Briggs RD, Pollard D, Tarasov L (2014) A data-constrained large ensemble analysis of Antarctic
890 evolution since the Eemian. *Quaternary Science Reviews* 103:91–115.
<https://doi.org/10.1016/j.quascirev.2014.09.003>
- 892 Broecker W, Putnam AE (2012) How did the hydrologic cycle respond to the two-phase mystery
interval? *Quaternary Science Reviews* 57:17–25.
<https://doi.org/10.1016/j.quascirev.2012.09.024>
- 894 Broecker WS (1998) Paleocean circulation during the Last Deglaciation: A bipolar seesaw?
Paleoceanography 13:119–121. <https://doi.org/10.1029/97PA03707>



- 896 Brown N, Galbraith ED (2016) Hosed vs. unhosed: interruptions of the Atlantic Meridional
Overturning Circulation in a global coupled model, with and without freshwater forcing.
898 Clim Past 12:1663–1679. <https://doi.org/10.5194/cp-12-1663-2016>
- Buizert C, Gkinis V, Severinghaus JP, et al (2014) Greenland temperature response to climate
900 forcing during the last deglaciation. *Science* 345:1177–1180.
<https://doi.org/10.1126/science.1254961>
- 902 CAPE-Last Interglacial Project Members (2006) Last Interglacial Arctic warmth confirms polar
amplification of climate change. *Quaternary Science Reviews* 25:1383–1400.
904 <https://doi.org/10.1016/j.quascirev.2006.01.033>
- Carlson AE, Clark PU (2012) Ice sheet sources of sea level rise and freshwater discharge during the
906 last deglaciation. *Rev Geophys* 50:RG4007. <https://doi.org/10.1029/2011RG000371>
- Clarke GKC, Bush ABG, Bush JWM (2009) Freshwater Discharge, Sediment Transport, and Modeled
908 Climate Impacts of the Final Drainage of Glacial Lake Agassiz. *Journal of Climate* 22:2161–
2180. <https://doi.org/10.1175/2008JCLI2439.1>
- 910 Collins WD, Bitz CM, Blackmon ML, et al (2006) The Community Climate System Model Version 3
(CCSM3). *Journal of Climate* 19:2122–2143. <https://doi.org/10.1175/JCLI3761.1>
- 912 Condron A, Winsor P (2012) Meltwater routing and the Younger Dryas. *Proc Natl Acad Sci USA*
109:19928–19933. <https://doi.org/10.1073/pnas.1207381109>
- 914 Crivellari S, Chiessi CM, Kuhnert H, et al (2018) Increased Amazon freshwater discharge during late
Heinrich Stadial 1. *Quaternary Science Reviews* 181:144–155.
916 <https://doi.org/10.1016/j.quascirev.2017.12.005>
- Cuzzone JK, Clark PU, Carlson AE, et al (2016) Final deglaciation of the Scandinavian Ice Sheet and
918 implications for the Holocene global sea-level budget. *Earth and Planetary Science Letters*
448:34–41. <https://doi.org/10.1016/j.epsl.2016.05.019>
- 920 de Beaulieu J-L, Reille M (1992) The last climatic cycle at La Grande Pile (Vosges, France) a new
pollen profile. *Quaternary Science Reviews* 11:431–438. [https://doi.org/10.1016/0277-
922 3791\(92\)90025-4](https://doi.org/10.1016/0277-3791(92)90025-4)
- Deschamps P, Durand N, Bard E, et al (2012) Ice-sheet collapse and sea-level rise at the Bølling
924 warming 14,600 years ago. *Nature* 483:559–564. <https://doi.org/10.1038/nature10902>
- Dome Fuji Ice Core Project Members:, Kawamura K, Abe-Ouchi A, et al (2017) State dependence of
926 climatic instability over the past 720,000 years from Antarctic ice cores and climate
modeling. *Sci Adv* 3:e1600446. <https://doi.org/10.1126/sciadv.1600446>
- 928 Dutt S, Gupta AK, Clemens SC, et al (2015) Abrupt changes in Indian summer monsoon strength
during 33,800 to 5500 years B.P.: INDIAN SUMMER MONSOON. *Geophys Res Lett* 42:5526–
930 5532. <https://doi.org/10.1002/2015GL064015>
- Dyke AS (2004) An outline of North American deglaciation with emphasis on central and northern
932 Canada. In: *Developments in Quaternary Sciences*. Elsevier, pp 373–424



- 934 Erb MP, Broccoli AJ, Clement AC (2013) The Contribution of Radiative Feedbacks to Orbitally
Driven Climate Change. *Journal of Climate* 26:5897–5914. <https://doi.org/10.1175/JCLI-D-12-00419.1>
- 936 Galbraith E, de Lavergne C (2019) Response of a comprehensive climate model to a broad range of
external forcings: relevance for deep ocean ventilation and the development of late
938 Cenozoic ice ages. *Clim Dyn* 52:653–679. <https://doi.org/10.1007/s00382-018-4157-8>
- 940 Ganopolski A, Rahmstorf S (2001) Rapid changes of glacial climate simulated in a coupled climate
model. *Nature* 409:153–158. <https://doi.org/10.1038/35051500>
- 942 Gherardi J, Labeyrie L, Mcmanus J, et al (2005) Evidence from the Northeastern Atlantic basin for
variability in the rate of the meridional overturning circulation through the last
deglaciation. *Earth and Planetary Science Letters* 240:710–723.
944 <https://doi.org/10.1016/j.epsl.2005.09.061>
- 946 Gherardi J-M, Labeyrie L, Nave S, et al (2009) Glacial-interglacial circulation changes inferred from
²³¹Pa/ ²³⁰Th sedimentary record in the North Atlantic region: MOC CHANGES INFERRED
FROM Pa/Th RECORDS. *Paleoceanography* 24:n/a-n/a.
948 <https://doi.org/10.1029/2008PA001696>
- 950 Giorgetta MA, Jungclaus J, Reick CH, et al (2013) Climate and carbon cycle changes from 1850 to
2100 in MPI-ESM simulations for the Coupled Model Intercomparison Project phase 5:
Climate Changes in MPI-ESM. *J Adv Model Earth Syst* 5:572–597.
952 <https://doi.org/10.1002/jame.20038>
- 954 Goosse H, Brovkin V, Fichfet T, et al (2010) Description of the Earth system model of intermediate
complexity LOVECLIM version 1.2. *Geosci Model Dev* 3:603–633.
<https://doi.org/10.5194/gmd-3-603-2010>
- 956 Gorbarenko SA, Shi X, Bosin AA, et al (2022) Relative sea level changes during the Last Glacial
Maximum and deglaciation (33–15 ka) inferred from the $\delta^{18}O$ records of planktic
958 foraminifera from the Sea of Japan. *Quaternary Science Reviews* 279:107386.
<https://doi.org/10.1016/j.quascirev.2022.107386>
- 960 Gregoire LJ (2010) Modelling the Northern Hemisphere Climate and Ice Sheets during the Last
Deglaciation
- 962 Gregoire LJ, Payne AJ, Valdes PJ (2012) Deglacial rapid sea level rises caused by ice-sheet saddle
collapses. *Nature* 487:219–222. <https://doi.org/10.1038/nature11257>
- 964 Gregoire LJ, Valdes PJ, Payne AJ (2015) The relative contribution of orbital forcing and greenhouse
gases to the North American deglaciation: DRIVERS OF N. AMERICAN DEGLACIATION.
966 *Geophys Res Lett* 42:9970–9979. <https://doi.org/10.1002/2015GL066005>
- 968 Grootes PM, Stuiver M, White JWC, et al (1993) Comparison of oxygen isotope records from the
GISP2 and GRIP Greenland ice cores. *Nature* 366:552–554.
<https://doi.org/10.1038/366552a0>
- 970 Harrison SP, Bartlein PJ, Izumi K, et al (2015) Evaluation of CMIP5 palaeo-simulations to improve
climate projections. *Nature Clim Change* 5:735–743. <https://doi.org/10.1038/nclimate2649>



- 972 Harrison SP, Braconnot P, Joussaume S, et al (2002) PMIP Workshop 4 : launching PMIP Phase II.
EOS 83:447–447
- 974 He C, Liu Z, Otto-Bliesner BL, et al (2021) Hydroclimate footprint of pan-Asian monsoon water
isotope during the last deglaciation. *Sci Adv* 7:eabe2611.
976 <https://doi.org/10.1126/sciadv.abe2611>
- He F (2011) Simulating transient climate evolution of the last deglaciation with CCSM 3. 72:
- 978 He F, Clark P (2022) Freshwater forcing of the Atlantic Meridional Overturning Circulation
revisited. <https://doi.org/10.17605/OSF.IO/NUQ2K>
- 980 He F, Shakun JD, Clark PU, et al (2013) Northern Hemisphere forcing of Southern Hemisphere
climate during the last deglaciation. *Nature* 494:81–85.
982 <https://doi.org/10.1038/nature11822>
- Huang J, Wan S, Li A, Li T (2019) Two-phase structure of tropical hydroclimate during Heinrich
984 Stadial 1 and its global implications. *Quaternary Science Reviews* 222:105900.
<https://doi.org/10.1016/j.quascirev.2019.105900>
- 986 Huang K-F, Oppo DW, Curry WB (2014) Decreased influence of Antarctic intermediate water in the
tropical Atlantic during North Atlantic cold events. *Earth and Planetary Science Letters*
988 389:200–208. <https://doi.org/10.1016/j.epsl.2013.12.037>
- Hughes ALC, Gyllencreutz R, Lohne ØS, et al (2016) The last Eurasian ice sheets – a chronological
990 database and time-slice reconstruction, DATED-1. *Boreas* 45:1–45.
<https://doi.org/10.1111/bor.12142>
- 992 Hurrell JW, Holland MM, Gent PR, et al (2013) The Community Earth System Model: A Framework
for Collaborative Research. *Bull Amer Meteor Soc* 94:1339–1360.
994 <https://doi.org/10.1175/BAMS-D-12-00121.1>
- Ivanovic RF, Gregoire LJ, Burke A, et al (2018) Acceleration of Northern Ice Sheet Melt Induces
996 AMOC Slowdown and Northern Cooling in Simulations of the Early Last Deglaciation.
Paleoceanography and Paleoclimatology 33:807–824.
998 <https://doi.org/10.1029/2017PA003308>
- Ivanovic RF, Gregoire LJ, Kageyama M, et al (2016) Transient climate simulations of the deglaciation
1000 21–9 thousand years beforepresent (version 1) – PMIP4 Core experiment design and
boundary conditions. *Geosci Model Dev* 9:2563–2587. <https://doi.org/10.5194/gmd-9-2563-2016>
1002
- Ivanovic RF, Gregoire LJ, Wickert AD, et al (2017) Collapse of the North American ice saddle 14,500
1004 years ago caused widespread cooling and reduced ocean overturning circulation: Ice
Collapse Caused Cooling ~14.5 ka. *Geophys Res Lett* 44:383–392.
1006 <https://doi.org/10.1002/2016GL071849>
- Joos F, Spahni R (2008) Rates of change in natural and anthropogenic radiative forcing over the
1008 past 20,000 years. *Proceedings of the National Academy of Sciences* 105:1425–1430.
<https://doi.org/10.1073/pnas.0707386105>



- 1010 Jouzel J, Masson-Delmotte V, Cattani O, et al (2007) Orbital and Millennial Antarctic Climate Variability over the Past 800,000 Years. *Science*. <https://doi.org/10.1126/science.1141038>
- 1012 Kageyama M, Merkel U, Otto-Bliesner B, et al (2013) Climatic impacts of fresh water hosing under Last Glacial Maximum conditions: a multi-model study. *Clim Past* 9:935–953.
1014 <https://doi.org/10.5194/cp-9-935-2013>
- Kapsch M, Mikolajewicz U, Ziemen F, Schannwell C (2022) Ocean response in transient simulations of the last deglaciation dominated by underlying ice-sheet reconstruction and method of meltwater distribution. *Geophysical Research Letters*.
1016 <https://doi.org/10.1029/2021GL096767>
1018
- Kapsch M-L, Mikolajewicz U, Ziemen FA, et al (2021) Analysis of the surface mass balance for deglacial climate simulations. *The Cryosphere* 15:1131–1156. <https://doi.org/10.5194/tc-15-1131-2021>
1020
- Klockmann M, Mikolajewicz U, Marotzke J (2018) Two AMOC States in Response to Decreasing Greenhouse Gas Concentrations in the Coupled Climate Model MPI-ESM. *J Climate* 31:7969–7984. <https://doi.org/10.1175/JCLI-D-17-0859.1>
1022
1024
- Klockmann M, Mikolajewicz U, Marotzke J (2016) The effect of greenhouse gas concentrations and ice sheets on the glacial AMOC in a coupled climate model. *Clim Past* 12:1829–1846. <https://doi.org/10.5194/cp-12-1829-2016>
1026
- Knutti R, Flückiger J, Stocker TF, Timmermann A (2004) Strong hemispheric coupling of glacial climate through freshwater discharge and ocean circulation. *Nature* 430:851–856.
1028 <https://doi.org/10.1038/nature02786>
1030
- Köhler P, Nehrbaas-Ahles C, Schmitt J, et al (2017) A 156 kyr smoothed history of the atmospheric greenhouse gases CO₂, CH₄, and N₂O and their radiative forcing. *Earth Syst Sci Data* 9:363–387.
1032 <https://doi.org/10.5194/essd-9-363-2017>
1034
- Lambeck K, Rouby H, Purcell A, et al (2014) Sea level and global ice volumes from the Last Glacial Maximum to the Holocene. *Proceedings of the National Academy of Sciences* 111:15296–15303. <https://doi.org/10.1073/pnas.1411762111>
1036
- Lea DW, Pak DK, Peterson LC, Hughen KA (2003) Synchronicity of Tropical and High-Latitude Atlantic Temperatures over the Last Glacial Termination. *Science* 301:1361–1364.
1038 <https://doi.org/10.1126/science.1088470>
1040
- Lippold J, Pöppelmeier F, Süfke F, et al (2019) Constraining the Variability of the Atlantic Meridional Overturning Circulation During the Holocene. *Geophysical Research Letters* 46:11338–11346. <https://doi.org/10.1029/2019GL084988>
1042
- Liu Z, Otto-Bliesner BL, He F, et al (2009) Transient Simulation of Last Deglaciation with a New Mechanism for Bolling-Allerod Warming. *Science* 325:310–314.
1044 <https://doi.org/10.1126/science.1171041>
1046



- 1048 Löffverström M, Lora JM (2017) Abrupt regime shifts in the North Atlantic atmospheric circulation over the last deglaciation. *Geophys Res Lett* 44:8047–8055.
<https://doi.org/10.1002/2017GL074274>
- 1050 Loulergue L, Schilt A, Spahni R, et al (2008) Orbital and millennial-scale features of atmospheric
1052 CH₄ over the past 800,000 years. *Nature* 453:383–386.
<https://doi.org/10.1038/nature06950>
- 1054 Lunt DJ, Dunkley Jones T, Heinemann M, et al (2012) A model–data comparison for a multi-model ensemble of early Eocene atmosphere–ocean simulations: EoMIP. *Clim Past* 8:1717–1736.
<https://doi.org/10.5194/cp-8-1717-2012>
- 1056 Lüthi D, Le Floch M, Bereiter B, et al (2008) High-resolution carbon dioxide concentration record
1058 650,000–800,000 years before present. *Nature* 453:379–382.
<https://doi.org/10.1038/nature06949>
- 1060 Lynch-Stieglitz J (2017) The Atlantic Meridional Overturning Circulation and Abrupt Climate Change. *Annu Rev Mar Sci* 9:83–104. <https://doi.org/10.1146/annurev-marine-010816-060415>
- 1062 Lynch-Stieglitz J, Adkins JF, Curry WB, et al (2007) Atlantic Meridional Overturning Circulation
1064 During the Last Glacial Maximum. *Science* 316:66–69.
<https://doi.org/10.1126/science.1137127>
- 1066 Ma Z-B, Cheng H, Tan M, et al (2012) Timing and structure of the Younger Dryas event in northern China. *Quaternary Science Reviews* 41:83–93.
<https://doi.org/10.1016/j.quascirev.2012.03.006>
- 1068 McCarthy G, Smeed D, Cunningham S, Roberts C (2017) Atlantic Meridonal Overturning Circulation. *MCCIP Science Review* 2017 7 pages. <https://doi.org/10.14465/2017.ARC10.002-ATL>
- 1070 McManus JF, Francois R, Gherardi J-M, et al (2004) Collapse and rapid resumption of Atlantic
1072 meridional circulation linked to deglacial climate changes. *Nature* 428:834–837.
<https://doi.org/10.1038/nature02494>
- 1074 Menviel L, Joos F, Ritz SP (2012) Simulating atmospheric CO₂, ¹³C and the marine carbon cycle during the Last Glacial–Interglacial cycle: possible role for a deepening of the mean remineralization depth and an increase in the oceanic nutrient inventory. *Quaternary Science Reviews* 56:46–68. <https://doi.org/10.1016/j.quascirev.2012.09.012>
- 1078 Menviel L, Timmermann A, Timm OE, Mouchet A (2011) Deconstructing the Last Glacial termination: the role of millennial and orbital-scale forcings. *Quaternary Science Reviews* 30:1155–1172. <https://doi.org/10.1016/j.quascirev.2011.02.005>
- 1080 Menviel L, Yu J, Joos F, et al (2017) Poorly ventilated deep ocean at the Last Glacial Maximum inferred from carbon isotopes: A data-model comparison study. *Paleoceanography* 32:2–17.
1082 <https://doi.org/10.1002/2016PA003024>
- 1084 Menviel LC, Skinner LC, Tarasov L, Tzedakis PC (2020) An ice–climate oscillatory framework for Dansgaard–Oeschger cycles. *Nat Rev Earth Environ* 1:677–693.
<https://doi.org/10.1038/s43017-020-00106-y>



- 1086 Muglia J, Schmittner A (2021) Carbon isotope constraints on glacial Atlantic meridional
1088 overturning: Strength vs depth. *Quaternary Science Reviews* 257:106844.
<https://doi.org/10.1016/j.quascirev.2021.106844>
- 1090 Muglia J, Schmittner A (2015) Glacial Atlantic overturning increased by wind stress in climate
1092 models: WIND STRESS AND GLACIAL AMOC. *Geophys Res Lett* 42:9862–9868.
<https://doi.org/10.1002/2015GL064583>
- 1092 Ng HC, Robinson LF, McManus JF, et al (2018) Coherent deglacial changes in western Atlantic Ocean
1094 circulation. *Nat Commun* 9:2947. <https://doi.org/10.1038/s41467-018-05312-3>
- 1094 Obase T, Abe-Ouchi A (2019) Abrupt Bølling-Allerød Warming Simulated under Gradual Forcing of
1096 the Last Deglaciation. *Geophys Res Lett* 46:11397–11405.
<https://doi.org/10.1029/2019GL084675>
- 1098 Oka A, Hasumi H, Abe-Ouchi A (2012) The thermal threshold of the Atlantic meridional overturning
1100 circulation and its control by wind stress forcing during glacial climate: THE THERMAL
THRESHOLD OF THE AMOC. *Geophys Res Lett* 39:n/a-n/a.
<https://doi.org/10.1029/2012GL051421>
- 1102 Otto-Bliesner BL, Brady EC (2010) The sensitivity of the climate response to the magnitude and
location of freshwater forcing: last glacial maximum experiments. *Quaternary Science
Reviews* 29:56–73. <https://doi.org/10.1016/j.quascirev.2009.07.004>
- 1104 Otto-Bliesner BL, Hewitt CD, Marchitto TM, et al (2007) Last Glacial Maximum ocean thermohaline
1106 circulation: PMIP2 model intercomparisons and data constraints. *Geophys Res Lett*
34:L12706. <https://doi.org/10.1029/2007GL029475>
- 1108 Park H-S, Kim S-J, Stewart AL, et al (2019) Mid-Holocene Northern Hemisphere warming driven by
Arctic amplification. *Sci Adv* 5:eaax8203. <https://doi.org/10.1126/sciadv.aax8203>
- 1110 Peltier WR (2004) GLOBAL GLACIAL ISOSTASY AND THE SURFACE OF THE ICE-AGE EARTH: The
ICE-5G (VM2) Model and GRACE. *Annu Rev Earth Planet Sci* 32:111–149.
<https://doi.org/10.1146/annurev.earth.32.082503.144359>
- 1112 Peltier WR, Argus DF, Drummond R (2015) Space geodesy constrains ice age terminal deglaciation:
1114 The global ICE-6G_C (VM5a) model: Global Glacial Isostatic Adjustment. *J Geophys Res Solid
Earth* 120:450–487. <https://doi.org/10.1002/2014JB011176>
- 1116 Pöppelmeier F, Baggenstos D, Grimmer M, et al (2023a) The Effect of Past Saturation Changes on
Noble Gas Reconstructions of Mean Ocean Temperature. *Geophysical Research Letters*
50:e2022GL102055. <https://doi.org/10.1029/2022GL102055>
- 1118 Pöppelmeier F, Jeltsch-Thömmes A, Lippold J, et al (2023b) Multi-proxy constraints on Atlantic
1120 circulation dynamics since the last ice age. *Nat Geosci* 16:349–356.
<https://doi.org/10.1038/s41561-023-01140-3>
- 1122 Rahmstorf S (2002) Ocean circulation and climate during the past 120,000 years. *Nature* 419:207–
214. <https://doi.org/10.1038/nature01090>



- 1124 Rahmstorf S (1999) Decadal Variability of the Thermohaline Ocean Circulation. In: Navarra A (ed) Beyond El Niño. Springer Berlin Heidelberg, Berlin, Heidelberg, pp 309–331
- 1126 Repschläger J, Zhao N, Rand D, et al (2021) Active North Atlantic deepwater formation during Heinrich Stadial 1. *Quaternary Science Reviews* 270:107145.
<https://doi.org/10.1016/j.quascirev.2021.107145>
- 1128 Riddick T, Brovkin V, Hagemann S, Mikolajewicz U (2018) Dynamic hydrological discharge
1130 modelling for coupled climate model simulations of the last glacial cycle: the MPI-DynamicHD model version 3.0. *Geosci Model Dev* 11:4291–4316.
<https://doi.org/10.5194/gmd-11-4291-2018>
- 1132 Roberts NL, Piotrowski AM, McManus JF, Keigwin LD (2010) Synchronous Deglacial Overturning
1134 and Water Mass Source Changes. *Science* 327:75–78.
<https://doi.org/10.1126/science.1178068>
- 1136 Roche DM, Renssen H, Paillard D, Levavasseur G (2011) Deciphering the spatio-temporal
complexity of climate change of the last deglaciation: a model analysis. *Climate of the Past*
7:591–602. <https://doi.org/10.5194/cp-7-591-2011>
- 1138 Roche DM, Renssen H, Weber SL, Goosse H (2007) Could meltwater pulses have been sneaked
1140 unnoticed into the deep ocean during the last glacial? *Geophys Res Lett* 34:L24708.
<https://doi.org/10.1029/2007GL032064>
- 1142 Roche DM, Wiersma AP, Renssen H (2010) A systematic study of the impact of freshwater pulses
with respect to different geographical locations. *Clim Dyn* 34:997–1013.
<https://doi.org/10.1007/s00382-009-0578-8>
- 1144 Romé YM, Ivanovic RF, Gregoire LJ, et al (2022) Millennial-Scale Climate Oscillations Triggered by
1146 Deglacial Meltwater Discharge in Last Glacial Maximum Simulations. *Paleoceanog and
Paleoclimatol* 37:. <https://doi.org/10.1029/2022PA004451>
- 1148 Roy K, Peltier WR (2018) Relative sea level in the Western Mediterranean basin: A regional test of
the ICE-7G_NA (VM7) model and a constraint on late Holocene Antarctic deglaciation.
Quaternary Science Reviews 183:76–87. <https://doi.org/10.1016/j.quascirev.2017.12.021>
- 1150 Schilt A, Baumgartner M, Schwander J, et al (2010) Atmospheric nitrous oxide during the last
1152 140,000years. *Earth and Planetary Science Letters* 300:33–43.
<https://doi.org/10.1016/j.epsl.2010.09.027>
- 1154 Schmidt GA, Jungclaus JH, Ammann CM, et al (2012) Climate forcing reconstructions for use in PMIP
simulations of the Last Millennium (v1.1). *Geosci Model Dev* 5:185–191.
<https://doi.org/10.5194/gmd-5-185-2012>
- 1156 Schmittner A, Lund DC (2014) Carbon isotopes support Atlantic meridional overturning circulation
1158 decline as a trigger for early deglacial CO₂ rise. *Ocean
Dynamics/Marine Archives/Millennial/D-O*
- 1160 Severinghaus JP, Brook EJ (1999) Abrupt Climate Change at the End of the Last Glacial Period
Inferred from Trapped Air in Polar Ice. *Science* 286:930–934.
<https://doi.org/10.1126/science.286.5441.930>



- 1162 Shakun JD, Clark PU, He F, et al (2012) Global warming preceded by increasing carbon dioxide
concentrations during the last deglaciation. *Nature* 484:49–54.
1164 <https://doi.org/10.1038/nature10915>
- Sherriff-Tadano S, Abe-Ouchi A, Yoshimori M, et al (2018) Influence of glacial ice sheets on the
1166 Atlantic meridional overturning circulation through surface wind change. *Clim Dyn*
50:2881–2903. <https://doi.org/10.1007/s00382-017-3780-0>
- 1168 Sherriff-Tadano S, Klockmann M (2021) PMIP contributions to understanding the deep ocean
circulation of the Last Glacial Maximum. *PAGES Mag* 29:84–85.
1170 <https://doi.org/10.22498/pages.29.2.84>
- Smith RS, Gregory JM (2009) A study of the sensitivity of ocean overturning circulation and climate
1172 to freshwater input in different regions of the North Atlantic: SENSITIVITY OF MOC TO
HOSING REGION. *Geophys Res Lett* 36:n/a-n/a. <https://doi.org/10.1029/2009GL038607>
- 1174 Smith RS, Gregory JM, Osprey A (2008) A description of the FAMOUS (version XDBUA) climate
model and control run. *Geosci Model Dev* 1:53–68. <https://doi.org/10.5194/gmd-1-53-2008>
1176
- Snoll B, Ivanovic RF, Valdes PJ, et al (2022) Effect of orographic gravity wave drag on Northern
1178 Hemisphere climate in transient simulations of the last deglaciation. *Clim Dyn*.
<https://doi.org/10.1007/s00382-022-06196-2>
- 1180 Stocker TF (1998) The Seesaw Effect. *Science* 282:61–62.
<https://doi.org/10.1126/science.282.5386.61>
- 1182 Sun Y, Knorr G, Zhang X, et al (2022) Ice sheet decline and rising atmospheric CO₂ control AMOC
sensitivity to deglacial meltwater discharge. *Global and Planetary Change* 210:103755.
1184 <https://doi.org/10.1016/j.gloplacha.2022.103755>
- Tarasov L, Dyke AS, Neal RM, Peltier WR (2012) A data-calibrated distribution of deglacial
1186 chronologies for the North American ice complex from glaciological modeling. *Earth and
Planetary Science Letters* 315–316:30–40. <https://doi.org/10.1016/j.epsl.2011.09.010>
- 1188 Tarasov L, Peltier WR (2002) Greenland glacial history and local geodynamic consequences.
Geophysical Journal International 150:198–229. <https://doi.org/10.1046/j.1365-246X.2002.01702.x>
1190
- Thornalley DJR, McCave IN, Elderfield H (2010) Freshwater input and abrupt deglacial climate
1192 change in the North Atlantic: DEGLACIAL FRESHWATER INPUT AND CLIMATE.
Paleoceanography 25:. <https://doi.org/10.1029/2009PA001772>
- 1194 Ullman DJ, Carlson AE, Hostetler SW, et al (2016) Final Laurentide ice-sheet deglaciation and
Holocene climate-sea level change. *Quaternary Science Reviews* 152:49–59.
1196 <https://doi.org/10.1016/j.quascirev.2016.09.014>
- Ullman DJ, LeGrande AN, Carlson AE, et al (2014) Assessing the impact of Laurentide Ice Sheet
1198 topography on glacial climate. *Clim Past* 10:487–507. <https://doi.org/10.5194/cp-10-487-2014>



- 1200 Valdes P (2011) Built for stability. *Nature Geosci* 4:414–416. <https://doi.org/10.1038/ngeo1200>
- 1202 Valdes PJ, Armstrong E, Badger MPS, et al (2017) The BRIDGE HadCM3 family of climate models: HadCM3@Bristol v1.0. *Geosci Model Dev* 10:3715–3743. <https://doi.org/10.5194/gmd-10-3715-2017>
- 1204 Veres D, Bazin L, Landais A, et al (2013) The Antarctic ice core chronology (AICC2012): an optimized multi-parameter and multi-site dating approach for the last 120 thousand years. *Clim Past* 9:1733–1748. <https://doi.org/10.5194/cp-9-1733-2013>
- 1208 Wang YJ, Cheng H, Edwards RL, et al (2001) A High-Resolution Absolute-Dated Late Pleistocene Monsoon Record from Hulu Cave, China. *Science* 294:2345–2348. <https://doi.org/10.1126/science.1064618>
- 1210 Weaver AJ, Eby M, Wiebe EC, et al (2001) The UVic earth system climate model: Model description, climatology, and applications to past, present and future climates. *Atmosphere-Ocean* 39:361–428. <https://doi.org/10.1080/07055900.2001.9649686>
- 1214 Wickert AD (2016) Reconstruction of North American drainage basins and river discharge since the Last Glacial Maximum. *Earth Surf Dynam* 4:831–869. <https://doi.org/10.5194/esurf-4-831-2016>
- 1216 Wilmes S-B, Green JAM, Schmittner A (2021) Enhanced vertical mixing in the glacial ocean inferred from sedimentary carbon isotopes. *Commun Earth Environ* 2:166. <https://doi.org/10.1038/s43247-021-00239-y>
- 1220 Yokoyama Y, Lambeck K, De Deckker P, et al (2000) Timing of the Last Glacial Maximum from observed sea-level minima. *Nature* 406:713–716. <https://doi.org/10.1038/35021035>
- 1222 Zhang X, Knorr G, Lohmann G, Barker S (2017) Abrupt North Atlantic circulation changes in response to gradual CO₂ forcing in a glacial climate state. *Nature Geosci* 10:518–523. <https://doi.org/10.1038/ngeo2974>
- 1224 Home | PMIP. <https://pmip.lsce.ipsl.fr/>. Accessed 8 Jun 2022
- 1226